TECHNISCHE UNIVERSITÄT MÜNCHEN

Abteilung für Neuroradiologie

(Direktor: Univ.- Prof. Dr. C. Zimmer)

Validation of dynamic contrast enhanced MR blood-brain barrier permeability measurements and prediction of hemorrhagic transformation in an adult rat model of ischemic stroke

Angelika Hoffmann

Vollständiger Abdruck der von der Fakultät für Medizin der Technischen Universität München zur Erlangung des akademischen Grades eines

Doktors der Medizin

genehmigten Dissertation.

Vorsitzender: Univ.-Prof. Dr. E. J. Rummeny

Prüfer der Dissertation: 1.   Univ.-Prof. Dr. C. Zimmer

                                           2.   Priv.-Doz. Dr. K. Holzapfel

Die Dissertation wurde am   28.02.2012   bei der Technischen Universität München eingereicht und durch die Fakultät für Medizin am   12.12.2012   angenommen.

Parts of this study have been published:

Hoffmann A, Bredno J, Wendland MF, Derugin N, Hom J, Schuster T, Su H, Ohara PT, Young WL, Wintermark M. Validation of In Vivo Magnetic Resonance Imaging Blood-Brain Barrier Permeability Measurements by Comparison With Gold Standard Histology. Stroke. 2011;42(7):2054-60.

Table of contents

List of abbreviations

ASL	Arterial Spin Labeling
ADC	Apparent Diffusion Coefficient
BBB	Blood-Brain Barrier
BBBP	Blood-Brain Barrier Permeability
CBF	Cerebral Blood Flow
CBV	Cerebral Blood Volume
CE-MRA	Contrast Enhanced-Magnetic Resonance Angiography
CT	Computer Tomography
CTA	CT Angiography
DCE	Dynamic Contrast Enhanced
DSC	Dynamic Susceptibility Contrast
DWI	Diffusion-weighted Imaging
Gd-DTPA	Gadolinium *D*iethylene*t*riamine*p*ent*a*cetate
GRE	Gradient Echo
HT	Hemorrhagic transformation
ICA	Internal Carotid Artery
ICH	Intracranial Hemorrhage
MCA	Middle Cerebral Artery
MRA	Magnetic Resonance Angiography
MRI	Magnetic Resonance Imaging
MTT	Mean Transit Time
PWI	Perfusion-weighted Imaging
PCT	Perfusion CT
ROI	Region of Interest
R1	longitudinal relaxation rate
SHR	Spontaneously Hypertensive Rats
SHT	Symptomatic Hemorrhagic Transformation
SI	Signal Intensity

TE   Echo Time

TI   Inversion Time

TOF-MRA   Time-of-Flight Magnetic Resonance Angiography

TR   Time to Repetition

TTP   Time–to-Peak

1   Introduction

Stroke is one of the leading causes of permanent disability and death in the world (Roger et al. 2011). According to the World Health Organization, 15 million people worldwide suffer from stroke annually.

It is important to distinguish ischemic from hemorrhagic stroke, which can be difficult clinically. Therefore, imaging – computed tomography (CT) or magnetic resonance imaging (MRI) - plays a central role in the evaluation of patients with acute stroke symptoms. The main goal in acute ischemic stroke treatment in the early phase is to rescue potentially salvageable ischemic brain tissue as fast as possible. Ischemic stroke is a highly treatable neuroemergency; early intravenous administration of recombinant tissue plasminogen activator (rtPA) remains the most beneficial proven intervention for emergency treatment of stroke. Several interventions, including intra-arterial administration of thrombolytic agents and mechanical interventions, show promise (Adams et al. 2007). CT or MR imaging offer important information to guide therapy, including the elimination of hemorrhage as a cause, the characterization of stroke location and subtype, as well as the assessment of tissue viability. The exact role of these additional pieces of information remains to be determined.

1.1 Imaging of acute stroke

A practical concept to understand the underlying causes and pathophysiology of ischemic stroke are the "four Ps" (parenchyma, pipe, perfusion and penumbra) proposed by Dr. Howard Rowley (Rowley 2001). Those "four Ps" can serve as an excellent guide to identify key elements of stroke with either CT or MR imaging.

1.1.1 Parenchyma

In about 85% of the cases, stroke is caused by ischemia, resulting in decreased blood supply to the brain. Causes can be cardiogenic, arteriosclerotic, lacunar, hemodynamic or idiopathic (Adams et al. 1993). In about 15%, stroke is hemorrhagic in nature and results from intracerebral hemorrhage (ICH), due to a

ruptured cerebral artery. The first step in the imaging work-up of a stroke patient is to determine whether the stroke is ischemic or hemorrhagic in nature.

Noncontrast CT is considered to be the gold standard for excluding ICH in the acute setting, although gradient recalled echo (GRE) MRI can also rule out ICH with high accuracy (Fiebach et al. 2004). FLAIR, a T2-weighted sequence with suppressed cerebrospinal fluid (CSF) signal, can be useful for detecting blood or gadolinium-based contrast agents especially in the CSF, e.g. subarachnoid hemorrhage. In terms of ischemic changes, FLAIR is sensitive to detect ischemic lesions adjacent to CSF such as subcortical lesions. However, they do not occur until approximately 6 hours after stroke onset.

Diffusion-weighted MRI (DWI) has been shown to be the most sensitive imaging modality in detecting early ischemic lesions in the setting of acute stroke (Chalela et al. 2007). In the first six hours after stroke onset, the overall sensitivity of DWI imaging is approximately 90% (Schellinger et al. 2010). Positive DWI findings without hyperintensity on FLAIR images indicate that the stroke has occurred less than 4.5 hours previously with a sensitivity of 62% and a specificity of 78% and can help to select patients with unknown stroke onset for thrombolysis (Thomalla et al. 2011). Contrary to DWI results, the overall sensitivity to detect early infarction signs with NCT within the first 6 hours of acute stroke ranges between 20% to 87% with a specificity of 56% to 100%, which reflects poor to moderate interobserver agreement (Wardlaw and Mielke 2005).

Additionally, the extent of the infarction plays an important role. Patients with a diffusion core volume smaller or equal to 70ml and treated with either intravenous thrombolysis or intraarterial therapy have a significantly better outcome than patients with a larger lesion (Sanak et al. 2006; Yoo et al. 2009). On NCT, if hypodensity is already well established in more than one third of the hemisphere, patients are likely not to profit from thrombolytic treatment and at risk of developing bad outcome.

1.1.2 Pipes

In the setting of stroke, intracranial and extracranial vessels need to be assessed for evidence of an intravascular thrombus or any other vascular pathology. NCT and FLAIR MR imaging can give some insight about vessel patency.

The hyperdense artery sign on NCT of patients represents acute thromboembolism. It is very specific (90-100%) and associated with poor outcome. This sign has a limited sensitivity of about 30% when using a slice thickness of 5 mm (Leys et al. 1992), but a higher sensitivity of 88% when using thin slice NCT (Kim et al. 2005). Furthermore, the thrombus length is of importance. If the thrombus length exceeds 8 mm, the likelihood of dissolving the clot with intravenous rtPA is very low, accounting for poor outcome (Riedel et al. 2011).

Analogous to the hyperdense atery sign on CT, MRI hyperintense artery signs have been described, such as the hyperintense artery sign using FLAIR imaging. The latter has been reported to have a sensitivity of 66% and specificity of 75% (Schellinger et al. 2005). If the hyperintense vessels are located proximal to the occlusion, they are likely the result of the intraluminal thrombus. Hyperintense vessels distal to the occlusion might be related to good collateral flow and have shown to be associated with smaller ischemic lesion volume on MRI and milder clinical severity (Lee et al. 2009).

Overall, CTA and MRA can detect arterial occlusions with a higher specificity and sensitivity than NCT or FLAIR imaging:

CT angiography (CTA) allows for rapid, non-invasive assessment of presence, extent and location of large intracranial and extracranial vessel occlusion with an overall accuracy of 95-99% (Lev et al. 2001; Bash et al. 2005; Tan et al. 2007). This information is of important prognostic value for acute ischemic stroke patients; e.g. patients with terminal carotid T occlusions, proximal middle cerebral artery (MCA) occlusion, MCA occlusions or tandem lesions tend to respond poorly to intravenous thrombolysis and might be candidates for intraarterial thrombolysis or mechanical clot retrieval. Moreover, CTA can determine the

patency and development of major collateral vessels, supplying the ischemic region (Miteff et al. 2009) and identify pathologies such as arterial dissection, or intracranial aneurysms, and might therefore prompt early alternative treatments.

Magnetic resonance angiography (MRA) offers a further method to evaluate the severity of vessel occlusion or stenosis as well as collateral flow. It primarily identifies the location of a thrombus and visualizes recanalization either spontaneously or in response to treatment. A typical stroke protocol includes time-of-flight MRA (TOF-MRA) or contrast-enhanced MRA (CE-MRA).

Overall, TOF-MRA shows similar sensitivity than CE-MRA (91.2% vs. 94.6%) in terms of detecting extracranial ICA stenoses greater or equal to 70% (Debrey et al. 2008). In differentiating between proximal occlusion with reduced flow and distal carotid-T occlusion, CE-MRA proved to be superior to TOF-MRA as a result of the ability to visualize arteries distal to the occluded segment (Alfke et al. 2011).

1.1.3 Perfusion and Penumbra

After having determined the presence, type and location of stroke, it is important to analyze the perfusion status, indicating the amount of cerebral blood flow arriving to a particular region of the brain. The occlusion site, but also its time course and potential collateral pathways, influence the viability of the cerebral tissue and consequently treatment options. Either CT or MRI can assess cerebral perfusion and help to determine and characterize the ischemic penumbra.

Perfusion CT (PCT) measures brain hemodynamics by tracking an intravenously injected bolus of ionidated contrast agent. In the setting of acute stroke, PCT is able to rapidly detect the size of hypoperfused brain regions (Wintermark et al. 2002). Using deconvolution methods as well as identification of the arterial input and venous outflow, perfusion parameters can be calculated: maps of cerebral blood flow (CBF), cerebral blood volume (CBV), and mean transit time (MTT). Cerebral blood flow (measured in milliliters per 100 g of brain tissue per minute) reflects the amount of blood flowing through each voxel in 1 minute. Cerebral blood volume (measured in milliliters per 100 g of brain tissue) reflects the blood

pool content of each pixel. Mean transit time (measured in seconds) designates the average time required for small volume of blood fluid to cross the capillary network in each pixel on the image. The relationship between CBV, MTT, and CBF is described by the following equation: CBF = CBV/MTT (Wintermark et al. 2001; Eastwood et al. 2003). If two of the three parameters are known, the third can be determined. Further time parameters such as time to peak (TTP) or Tmax can also be calculated. In stroke patients, PCT can grade the degree of hypoperfusion and distinguish tissue that will inevitably die (infarct core) from tissue that may either die or survive (ischemic penumbra). Acute arterial occlusion reduces distal cerebral perfusion pressure and is thus most severe in the center of infarction, the infarct core. The perfusion pressure reduction in the core is severe enough to overwhelm cerebrovascular autoregulation, which results in a decrease of CBV. However, in the penumbra, autoregulation is preserved and induces dilatation of the surrounding capillaries in an attempt to maintain adequate circulation. Vasodilatation and recruitment of collaterals maintain or increase CBV in the penumbral tissue. MTT is prolonged in the infarct core and the penumbra as a result of the decreased perfusion pressure (Table 1).

Table 1: Change of perfusion parameters in acute ischemic stroke in penumbra and infarct core

	Time parameter	CBF	CBV
Ischemic penumbra	⇑	⇓	normal or ⇑
Infarct core	⇑	⇓	⇓

The exact parameters and thresholds, which best characterize the ischemic core and penumbra are still a topic of debate and complicated by the fact that different scanner manufacturers use different algorithms to calculate perfusion parameters (Dani et al. 2011).
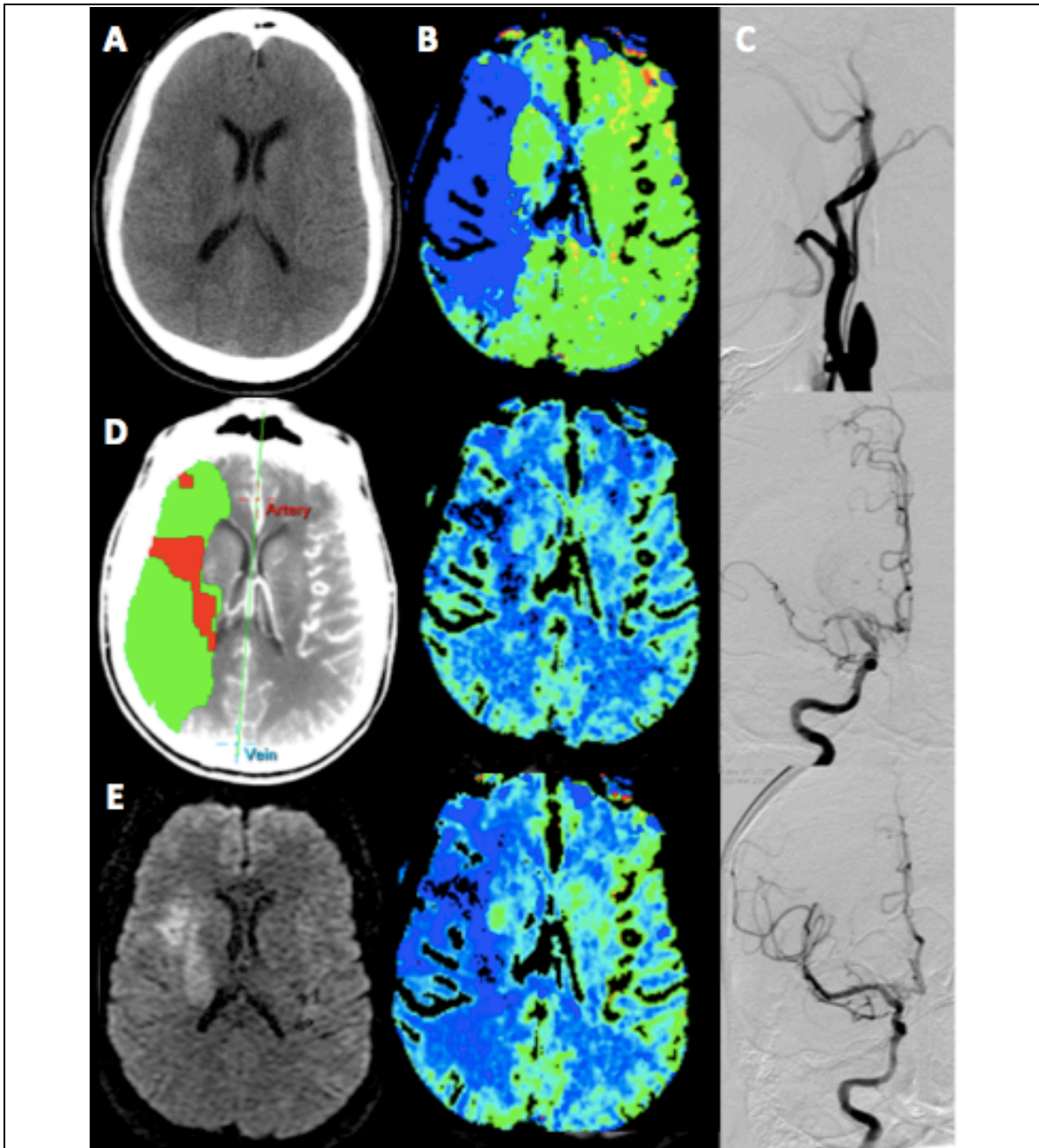
Figure 1: Sample case: 49-year old man presented with left hemiparesis and imaging was performed 1h after symptom onset. **A:** NCT images show no intracranial hemorrhage **B:** PCT maps (from top to bottom: MTT, CBV, CBF) show increased MTT and decreased CBV and CBF in the right frontal and temporal lobes. **D:** The region of decreased CBV corresponds to the infarct core, whereas the surrounding mismatch region of prolonged MTT represents the ischemic penumbra**.** Patient is treated with IV rtPA followed by mechanical thrombectomy. **C**: DSA images (from top to bottom) 2h after system onset show occlusion of the right internal carotid artery and of the M1 segment of the right MCA before and after recanalization with Merci retriever system and stent. **F**: Follow-up DWI scan shows small infarct volume corresponding to the infarct core determined with PCT. Patient shows favorable clinical outcome at discharge and at 90 days.

Two MRI methods can be used to assess brain perfusion: dynamic susceptibility contrast-enhacend imaging (DSC-PWI) and arterial spin labeling (ASL). ASL is not yet performed routinely in clinical practice. However, especially in patients with contraindications to Gd-based contrast agent, ASL perfusion measurements are a promising tool.

DSC-PWI relies on the measurement of T2 or T2* signal decrease due to the susceptibility effect of intravascular MR contrast agents during the first pass through the cerebral capillary bed (Grandin 2003). These signal changes in the cerebral tissue are tracked to create voxel-based hemodynamic time-intensity curves (Rosen et al. 1990). CBF, CBV, and MTT maps can be generated from these time-intensity curves (Smith et al. 2000). Compared to PCT, this step is more complex with DSC since the relationship between signal intensity and gadolinium concentration proves to be not linear (Kiselev 2001). How to determine the criteria that best characterize the ischemic region, is a central topic of ongoing research (Kane et al. 2007; Christensen et al. 2009). The volume difference between DWI lesions and hypoperfused tissue on PWI can be used to estimate the ischemic penumbra (Jansen et al. 1999; Schlaug et al. 1999). The DWI lesion thereby reflects the irreversibly damaged infarct core, while the PWI lesion shows the complete area of hypoperfusion. Applying the PWI/DWI mismatch in some clinical studies has been shown to be helpful in identifying patients who may benefit from thrombolysis (Hacke et al. 2005; Albers et al. 2006; Furlan et al. 2006; Davis et al. 2008), while others yielded negative results (Davis et al. 2008; Hacke et al. 2009). Automated image analysis software to detect the mismatch shows promise for decreasing interobserver variation (Lansberg et al. 2011).

1.1.4 Permeability

Permeability shows promise to be added as 5th P of the underlying causes and pathophysiology of stroke because it has the potential to evaluate the risk of hemorrhagic transformation with high sensitivity.

Symptomatic hemorrhagic transformation (SHT) is a serious complication of acute ischemic stroke and associated with worse clinical outcome (Berger et al. 2001). Although the definition and the magnitude of the SHT problem are still under debate (Saver 2007; Gumbinger et al. 2012), there is consensus that minimizing the occurrence of SHT is of great importance. Data from major acute stroke trials using intravenous rtPA reported SHT rates from 2.4% to 8.8% (Marler and al. 1995; Hacke et al. 1998; Clark et al. 1999; Hill and Buchan 2005; Hacke et al. 2008; Hacke et al. 2009; Shobha et al. 2011). Acute stroke trials applying mechanical revascularization or approaches combining intravenous and intraarterial thrombolysis showed that SHT occured in 8% to 9.9% of cases (Furlan et al. 1999; Smith et al. 2005; Broderick and IMS 2007; Smith et al. 2008). These results demonstrate that safety remains an important issue in acute stroke treatment, especially with regard to extended reperfusion therapy.

Increased blood-brain barrier permeability (BBBP) has been associated with an increased risk of SHT (Wang and Lo 2003) and could add valuable information to the evaluation of patients at risk of developing this complication. BBBP imaging shows promise to predict SHT based on either CT or MRI imaging (Knight et al. 1998; Neumann-Haefelin et al. 2002; Kassner et al. 2005; Bang et al. 2007; Bisdas et al. 2007; Aviv et al. 2009) and might possibly enable a transition from using a fixed therapeutic time window for rtPA administration to treatment decisions based on individual patient risk (Kassner et al. 2011). This could be of particular value in patients with unknown stroke onset or "wake-up" stroke, as well as potentially guide treatment decision in acute stroke therapies such as the bridging therapy (combined intravenous and intraarterial treatment). The latter has shown a favorable outcome in e.g. patients with an isolated MCA occlusion (Rouchaud et al. 2011), but is associated with a higher risk of symptomatic hemorrhage.
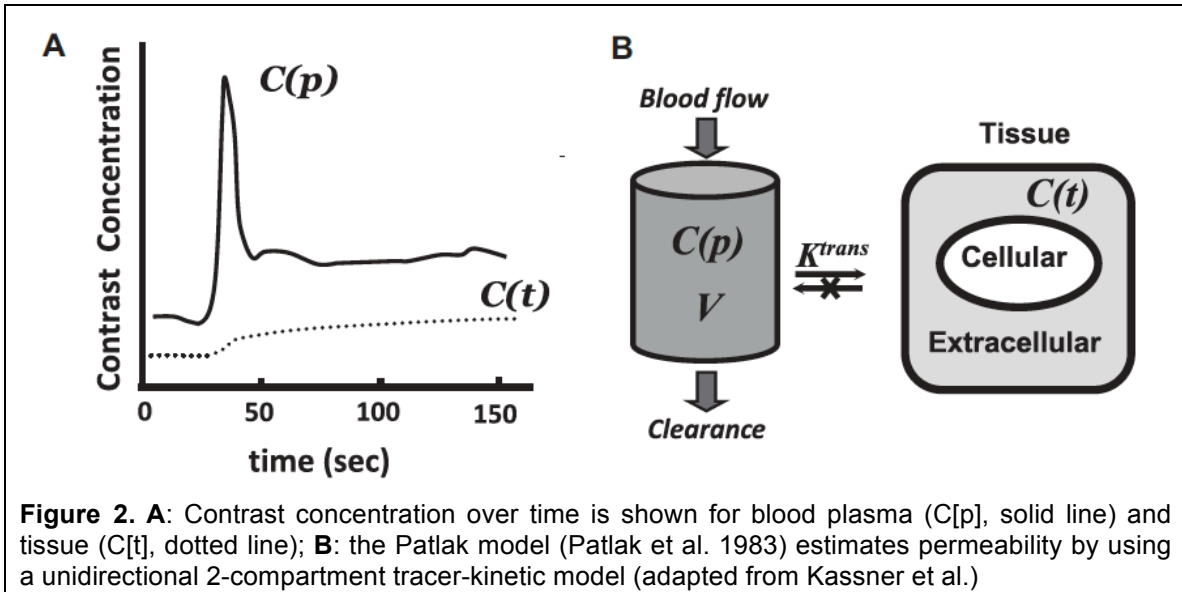
Pathophysiology of hemorrhagic transformation

HT is a multifactorial phenomenon (Wang and Lo 2003), with damage to the blood-brain barrier (BBB) and subsequent vascular leakage being considered as

13

a major contributing mechanism (Lyden and Zivin 1993; Lapchak 2002). HT can occur spontaneously, but is more often triggered by reperfusion (Wang and Lo 2003). Oxidative stress occurs very early after ischemia and its effect is worsened by reperfusion. This effect causes damage to lipid-rich membranes in the BBB, and consequently leads to vascular leakage and possibly vascular disruption in ischemic brain tissue (Chan 1994; Gursoy-Ozdemir et al. 2004). Additionally, oxidative stress stimulates inflammatory cytokine production and protease secretion by microglia, infiltrating leucocytes and resident cells of the neurovascular unit (Inoue et al. 2001; Haddad 2002). As these neuroinflammatory mechanisms become activated, alterations in cytokine profiles, adhesion-molecule expression and tight junction components mediate further vascular leakage (Wang and Lo 2003). Although many proteases are expressed in the brain under normal and ischemic conditions, both clinical (Rosell et al. 2006) and experimental (Rosenberg et al. 1996; Planas et al. 2001) studies suggest that the matrix metalloproteinase family and the tPA system play a central role in activating the proteolysis cascade.

Pharmacokinetic models to access blood-brain barrier permeability

In several diseases, including stroke, the BBB becomes permeable (Hawkins and Davis 2005) and contrast agent leakage may occur. Quantitative measurements of BBB permeability can be obtained by applying pharmacokinetic models to dynamic contrast enhanced imaging data, which are mainly based on compartmental models. All models measure the amount of tracer or contrast agent in a voxel of interest and the change over time in a time-concentration curve (TCC). Most often the TCCs are analyzed in comparison to a reference curve for blood plasma data (Figure 2A). One model, the Patlak model, (Patlak et al. 1983; Patlak and Blasberg 1985) is a unidirectional two-compartment model. It offers a simple quantitative measure of permeability (Lin et al. 2007), independent of contrast agent inflow while avoiding the complexity of other model-based approaches (Figure 2B).

Figure 2. A: Contrast concentration over time is shown for blood plasma (C[p], solid line) and tissue (C[t], dotted line); **B**: the Patlak model (Patlak et al. 1983) estimates permeability by using a unidirectional 2-compartment tracer-kinetic model (adapted from Kassner et al.)

For the Patlak analysis, the TCC(t) describing the observed amount of contrast agent in a perfused voxel is modeled as the sum of intravascular and interstitial, extravasated contrast agent.

$$TCC(t) = CBV \cdot c_p(t) + K_1 \int_0^t c_p(\tau) d\tau$$

The intravascular concentration c_p is multiplied with the cerebral blood volume CBV and estimates the attenuation that results from intravascular contrast agent. The amount of contrast agent which has permeated through the BBB is modeled as a fraction of all contrast having passed through the voxel since the start of the acquisition, and this fraction is interpreted as blood-to-brain transfer constant K_1 (Ewing et al. 2003; Lin et al. 2007).

Pharmacokinetic models to access BBB integrity, like the Patlak model, which were originally developed for nuclear tracer imaging (Patlak and Blasberg 1985; Saha et al. 1994), can also be applied to perfusion-CT data or dynamic contrast enhanced MRI data.

As indicated above, PCT relies on intravenous injection of an iodinated contrast agent and measures the attenuation coefficient (Hounsfield units) as a function of time on a voxel basis. PCT acquisitions should extend at least 210 seconds, in

order to generate accurate permeability values (Hom et al. 2009). A prospective study had promising predictive power for HT in general, but was unable to grade the degree of hemorrhage (Aviv et al. 2009). Another study showed promising results for prediction of the development of SHT and malignant edema considering BBB permeability admission data, t-PA administration and age ≥ 65 years (Hom et al. 2011).

Dynamic contrast enhanced MRI (DCE MRI) involves intravenous bolus injection of a gadolinium contrast agent followed by T1-weighted GRE imaging of the brain repeated over several minutes. A linear relationship between MR signal intensity and time can be observed, the slope of which has been related to blood-brain barrier permeability. Elevations in BBB permeability can be observed with DCE-MRI, even in the absence of visible postcontrast T1-weighted enhancement in patients who subsequently hemorrhaged (Kassner et al. 2005). One study suggested that DCE acquisition time must range from contrast injection to at least 3 minutes and 30 seconds in order to differentiate between HT and non-HT patients (Vidarsson et al. 2009). Further studies have outlined the promise of using DSC MR imaging as surrogate marker for BBB permeability to predict hemorrhagic transformation (Bang et al. 2007).

Blood-brain barrier permeability measurements in animal studies

Neuroimaging markers for HT were first reported in rats subjected to transient middle cerebral artery (MCA) occlusion. An early parenchymal contrast enhancement on T1-weighted images after the application of Gd-containing contrast agents was observed in areas that developed HT (Knight et al. 1998).

The pathophysiological correlate is most likely a loss of basal lamina in cerebral microvessels, which allows the extravasation of contrast medium molecules into the extravascular space (Hamann et al. 1999). Different approaches have been applied to validate BBB permeability imaging by assessing damage to various constituents of the BBB or by examining the extravasation of various molecules through the damaged BBB (Kuroiwa et al. 1985; Belayev et al. 1996; Ewing et al. 2003; Fenstermacher et al. 2003; Nagaraja et al. 2007; Burggraf et al. 2008).

2 Aims

Symptomatic hemorrhagic transformation is associated with a worse clinical outcome and occurs more frequently in extended reperfusion therapies. Developing an imaging tool to access the risk of SHT in acute ischemic stroke, patients could add valuable information for patients at risk of this complication and potentially guide treatment decisions. Blood-brain barrier permeability imaging might be a promising tool to predict hemorrhagic transformation.

BBBP measurements using dynamic contrast-enhanced MRI relies on applying a mathematical model to the time-signal curves of an intravascular, partly permeating tracer recorded on the images. A mathematical model is always a simplified representation of the reality summarized by an equation. As long as assumptions underlying the model are respected, results should follow theory, but cannot necessarily be considered as definite; validation against a gold standard is required.

Thus the aims of this thesis were to

1) validate BBBP measurements in a rat model of ischemic stroke using a relatively simple and frequently applied mathematical model, the Patlak model (Patlak et al. 1983; Patlak and Blasberg 1985), in order to provide quantitative values of blood-brain barrier permeability in rats with strokes induced by intraluminal filament MCA occlusion; and to

2) analyze the predictive value of BBBP measurements in terms of hemorrhagic transformation.

3 Material and Methods

3.1 Study design

The experimental animals were cared for in accordance with the Animal Welfare Act. Moreover, the experiments were conducted in compliance with our institutional guidelines for animal research and with the approval of the University of California San Francisco Committee on Animal Research.

Spontaneously hypertensive (SHR) male rats and Wistar male rats weighing 220 to 280 grams (Charles River laboratory, Hollister, CA for Wistar rats and Portage, MI for SHR rats) became subjected to a 2h filament occlusion of the right middle cerebral artery. The two different breeds, Wistar and SHR rats, were selected so that the same 2h MCA occlusion could result in different degrees of BBB disruption and of hemorrhagic transformation, despite similar infarct size at 24 hours post-reperfusion to brain tissue. MR imaging was obtained during occlusion, as well as 4h and 24h after reperfusion.

All experiments – surgery and MR imaging - were performed with the animals being anesthetized. Anesthesia was induced (3.5%) and maintained (2%) by isoflurane.

Immediately after the 24-hour MRI scan, the animal was injected with Evans blue (Sigma Chemical Co, St. Louis, Missouri, USA; 0.6ml of a 2% solution in saline), which circulated for 30min. After the circulation period, the animals were euthanized by decapitation, the brain was quickly removed and prepared for histological processing.

3.2 Animal Surgery

Reversible middle cerebral artery occlusion was performed according to a previously described technique (Longa et al. 1989). In brief, we inserted a precoated suture (4.0, Ethicon) through the external carotid artery (ECA) into the internal carotid artery (ICA). The suture was advanced 18-23mm past the ECA-ICA bifurcation to occlude the MCA. MCA occlusion and associated ischemic injury were confirmed during occlusion by perfusion- and diffusion-weighted MRI. Reperfusion of the MCA territory was achieved by withdrawal of the suture 2 hours after occlusion.

3.3 MR Imaging

The MRI was performed with a 2T Bruker Omega CSI system (Bruker Instruments Inc., Fremont, CA) equipped with Acustar S-150 self-shielded gradients (+/- 20G/cm, 15cm inner diameter). The animals were placed supine on a plastic support with ear and bite bars to minimize head motion during breathing. The head was inserted into a custom 5.5-cm diameter birdcage transmit–receive imaging coil. A water-recirculating warming pad was wrapped around the animal below its neck to maintain body temperature at 37ºC, as monitored by an intrarectal thermocouple.

The MRI protocol was the same at each time point (during occlusion, as well as 4h and 24h after reperfusion) and is summarized in Table 2. All images were obtained in the coronal plane.

Table 2: **Imaging protocol.** Images according to this protocol were taken during occlusion, 4h, and 24h post reperfusion. All images were obtained as 8 consecutive 2mm slices (if not otherwise specified), with an image matrix size of 128x128 pixels.

	TR/TE [ms]	Ave-rage	Field of view [mm^2]	Flip Angle	Additional Information
T1	500/10	2	38.4	90°-180° (spin echo)	Localizer
T2	2500/80	2	38.4	90°-180° (spin echo)	
DWI	2500/80	2	38.4	90°-180° (spin echo)	b factor=1030s/mm^2 applied along z-axis
T2* GRE	320/20	4	38.4	30°	
snapshot FLASH inversion recovery	3/3.5	1	38.4	10°	TI incremented from 100 to 2850 ms; Quantification of T1-values
Permeability T1 DCE (dynamic contrast enhancement)	50/3.5	1	38.4	90°	16 sets of images, 1pre- &15 post contrast sets; images repeated every 1min 56sec; short bolus of 0.3mmol/kg Gd-DTPA (Magnevist; Bayer)
Perfusion T2* DSC (dynamic susceptibility enhancement)	1000/17	1	50	(echo planar)	second short bolus of 0.3mmol/kg; 32 images acquired at 1s interval; 1 slice

At first, a scout T1 sequence of 8 consecutive 2mm slices was acquired with TR / TE = 500 / 10 ms; image matrix 128x128 pixel; field of view $(38.4 mm)^2$. The sequence was performed twice and averaged to increase the signal to noise ratio. This sequence was used to confirm the correct positioning of the animal in the magnet. Coverage ranged from the olfactory bulb to the floculli of the cerebellum (Figure 3).
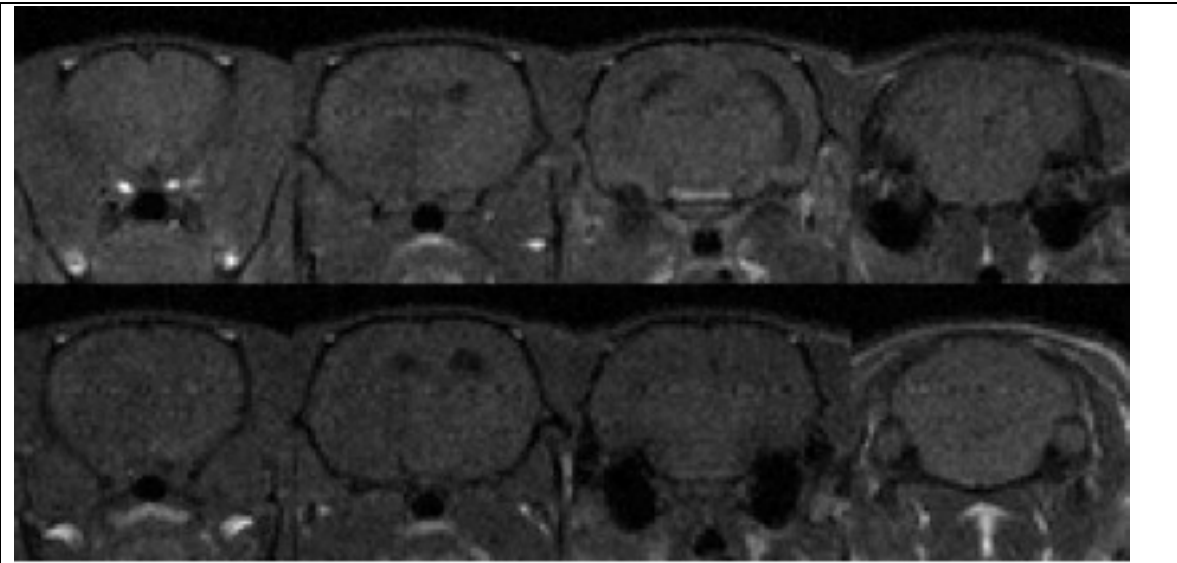

Figure 3: T1-weighted images are used to determine the positioning of the animal in the scanner

Multislice T2-weighted (Figure 4) and DWI (b-factor=1030s/mm^2 applied along the Z-axis) spin echo images were acquired with TR/TE=2500/80ms using the same imaging geometry and average for both sequences.
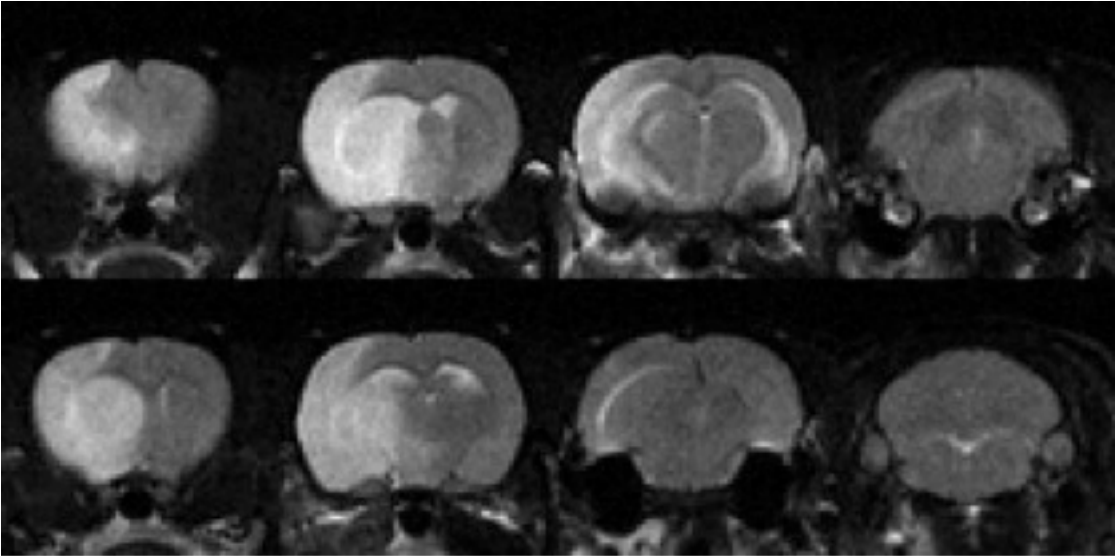
Figure 4: T2-weighted images are used to identify the brain anatomy. Here 24h post reperfusion images show the hyperintense ischemic lesion with ispilateral swelling and midline shift.

Aiming at detecting hemorrhages in-vivo, T2*-weighted gradient echo (GRE) images were acquired with TR / TE = 230 / 20 ms at a flip angle of 30º with 4 averages.

Quantitative pre-contrast T1-values (Figure 5) were measured using inversion recovery fast centric ordered gradient echo images with TI incremented from 100 to 2850 ms and TR / TE = 3 / 1.5 ms at a flip-angle of 10 degrees and delay of 10s between images to assure complete relaxation. These sequences were repeated at 4 contiguous slices that covered the area of interest most often affected by an MCA occlusion. R1 maps (where R1 = 1/T1) were calculated for each slice location by fitting the pixel values to the signal equation:

$SI(TI) = a - b*exp(-TI*R1)$.

Figure 5: Quantitative T1 maps are used to determine the contrast agent concentration of post-contrast images.

In order to achieve quantitative hemodynamic measurements of cerebral perfusion and permeability, two boluses of 0.3 mmol/kg animal body weight of Gd-DTPA (Magnevist; Bayer) were injected via a tail vein catheter. The first bolus of contrast was administered to measure permeability and served as a pre-load bolus for the perfusion scans, performed with a second bolus of contrast. As shown previously (Wintermark et al. 2005), this preloading minimizes the effect of contrast leakage for the perfusion imaging.

BBB permeability was imaged by dynamic GRE imaging after the first pass of the contrast agent bolus using TR / TE = 50 / 3.5 ms with a flip-angle 90°. 1 pre and 15 post contrast images were acquired with one image acquired every 1s and 56min (Figure 6). In post-processing the changes in signal intensity during dynamic GRE were converted to changes in R1 (R1=1/T1, ΔR1 is in principle proportional to concentration while Δsignal is not) using the relationship:

ΔR1 = -ln[1-(1-exp(-TR*R1pre))*SIpost/SIpre)/TR] – R1pre

in which SI pre- and post- contrast are pixel signal intensities obtained during dynamic GRE sequence and R1 pre was obtained from the R1 maps described above.
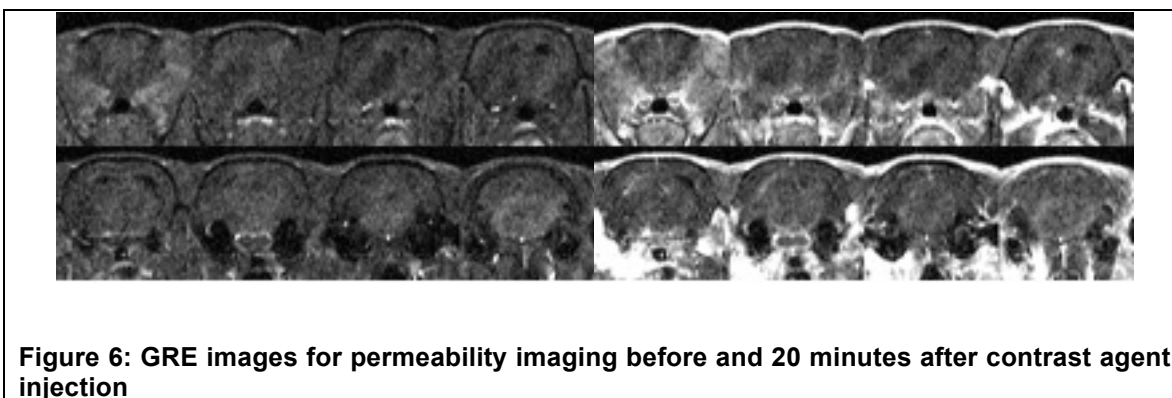

Figure 6: GRE images for permeability imaging before and 20 minutes after contrast agent injection

Perfusion sensitive MRI was performed via gradient-echo echo planar imaging (EPI). A set of 32 echo planar images was acquired at 1 s intervals with:

TE = 17 ms, FOV = 50 mm^2 matrix = 128 x 128 and slice thickness = 2 mm. This single slice position was selected to cover the center of the infarction territory. Four baseline images were acquired before contrast was injected (Figure 7).

Raw $\Delta R2^*$ maps were calculated using $\Delta R2^* = - \log [S(t)/S(0)] / TE$, where S(0)=average signal from the four baseline images and S(t)=MRI signal of subsequent images obtained during the first pass of contrast agent. $\Delta R2^*$ values were assumed proportional to contrast concentration.
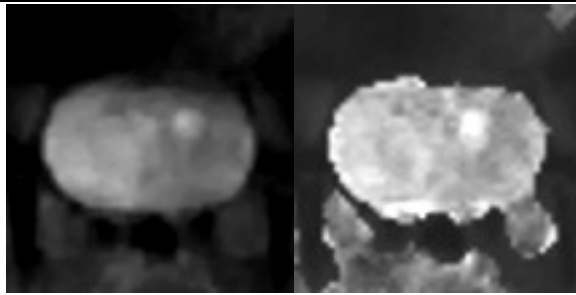

Figure 7: Perfusion-sensitive images before and 20 seconds after contrast agent injection during the passage of the first pass of contrast agent. Images have been processed to present contrast agent as increase in intensity.

3.4 Image Processing

The brain parenchymal tissue was segmented by intensity thresholding on the T2-weighted images. All subsequent processing was limited to the voxels belonging to the brain parenchymal tissue mask as determined by segmentation.

Perfusion maps were computed using commercially available software (Brain Perfusion, Extended Brilliance Workspace, Philips Healthcare, Cleveland, OH, USA) that was modified internally and tailored for the purposes of this research project (Figure 8). This software relies on the central volume principle, which has proved to be the most accurate for low injection rates of iodinated contrast material (Wintermark et al. 2001). After motion correction and noise reduction by an anisotropic, edge-preserving spatial filter, the software applies curve fitting by least mean squares to obtain mathematical descriptions of the time-density

curves for each pixel. The cerebral blood volume (CBV) map is calculated from the area under the time-density curves compared to a similarly obtained venous reference curve (Ladurner et al. 1976). A closed-form deconvolution is then applied to calculate the mean transit time (MTT) map (Axel 1983). The deconvolution operation requires a reference arterial input function that was manually selected. Such closed-form deconvolution provides MTT maps even for animal data with a mean transit time in brain tissue (1.5 s) close to the sampling rate (1s), which is a challenge for all perfusion algorithms. The cerebral blood flow (CBF) was computed as: CBF = CBV/MTT.
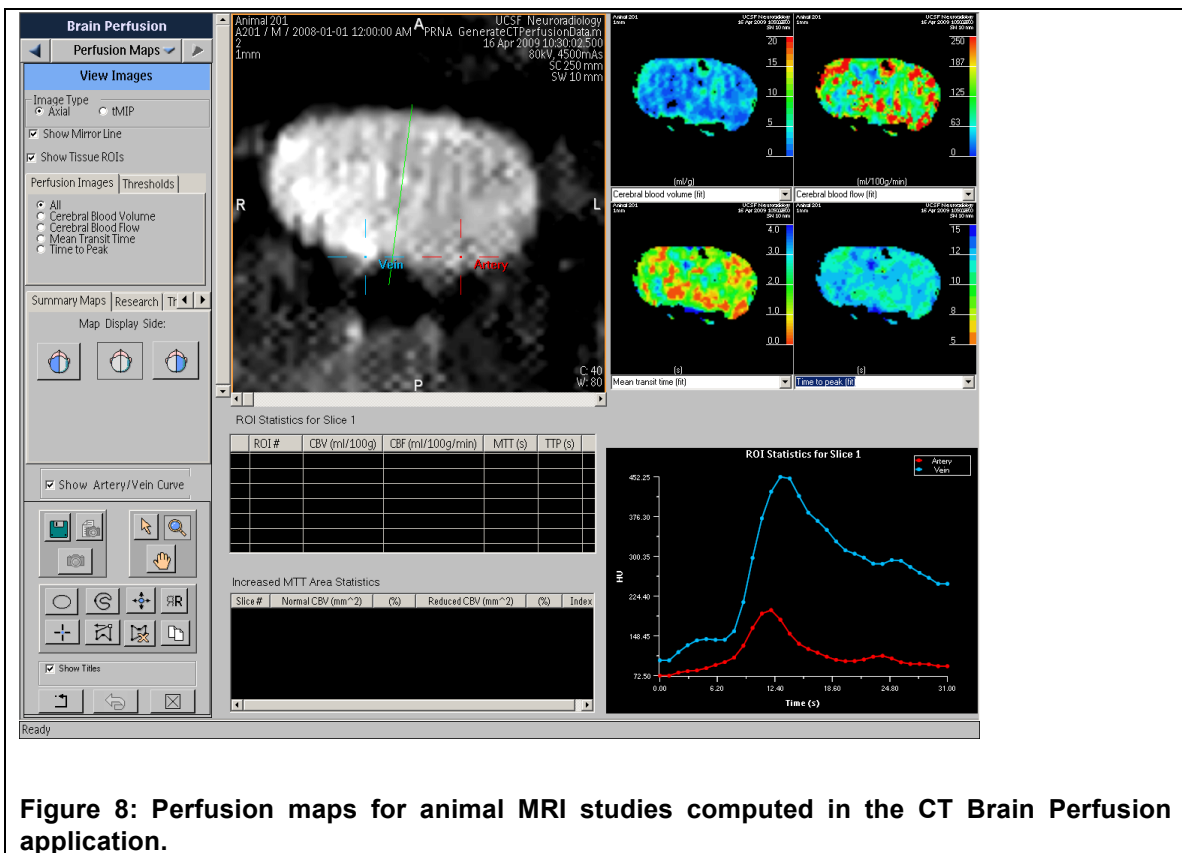

Figure 8: Perfusion maps for animal MRI studies computed in the CT Brain Perfusion application.

For the computation of permeability maps, the superior sagittal sinus was manually selected to provide the reference time-concentration curve for the intravascular contrast agent concentration (Figure 9).
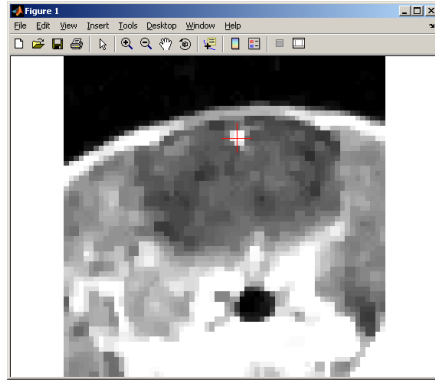
Figure 9: Definition of a reference vessel for the permeability analysis.

Permeability maps were computed by Patlak analysis (Patlak et al. 1983; Patlak and Blasberg 1985), which provides an estimation of a local CBV along with the blood-to-brain transfer constant k_1.

The method is based on the T2 image for a semi-automated brain delineation and uses this geometric information for the processing of dynamic GRE data (Figure 10).

Figure 10: A threshold segmentation in the selected brain ROI allows to create the brain mask.

The analysis included an additional stabilizing step where the area under the reference curve was scaled such that a target median CBV of 3ml/100g was obtained in the contralateral hemisphere for all animals at all time points (Figure 11).

Figure 11: Blood-to-brain transfer constant K_1 ($^{ml}/_{min \cdot 100g}$) from the unilateral model with intravascular compartment (stabilized Patlak analysis).
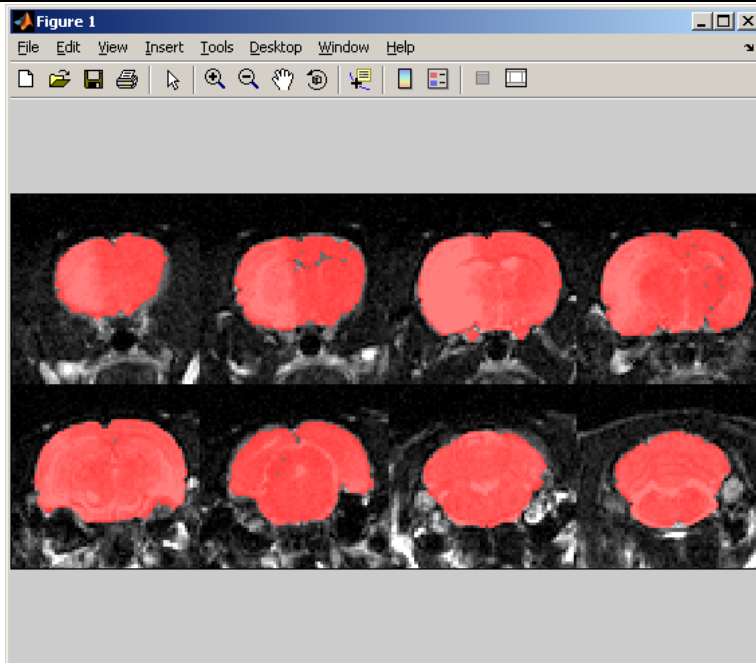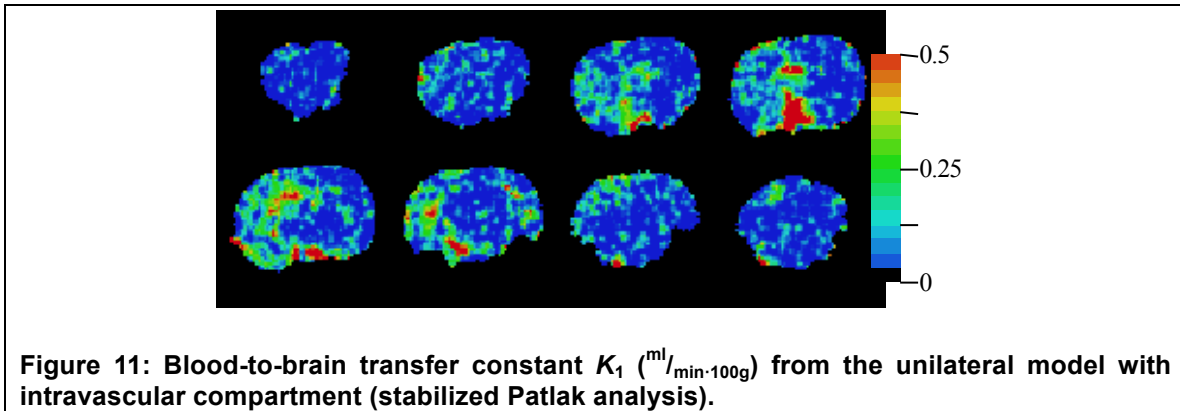
3.5 Histopathology

Frozen tissue sections of 50μm were cut on a cryostat (Leica Microsystems, Wetzlar, Germany) from Bregma -5mm to +2mm (George Paxinos 2005) covering all regions possibly affected by infarction. Every 500μm, two sections were collected and used for Cresyl-violet staining and fluorescent microscopy analyses.

3.6 Image Analysis: Infarction and Hemorrhage

Sections stained with Cresyl-violet were examined microscopically with varying magnifications to delineate infarction and to identify different types of hemorrhagic transformation.

The infarction was identified on the Cresyl-violet section on light microscopy as a region of pallor that contained shrunken cell bodies characteristic of neuronal cell death.

Macroscopic hemorrhage was defined as blood visible without magnification and confirmed by higher magnification (20x). Microscopic hemorrhage was defined as blood visible only by microscopy (20x) (Ding et al. 2005) showing tissue characteristics of a petechial bleed (Figure 12).
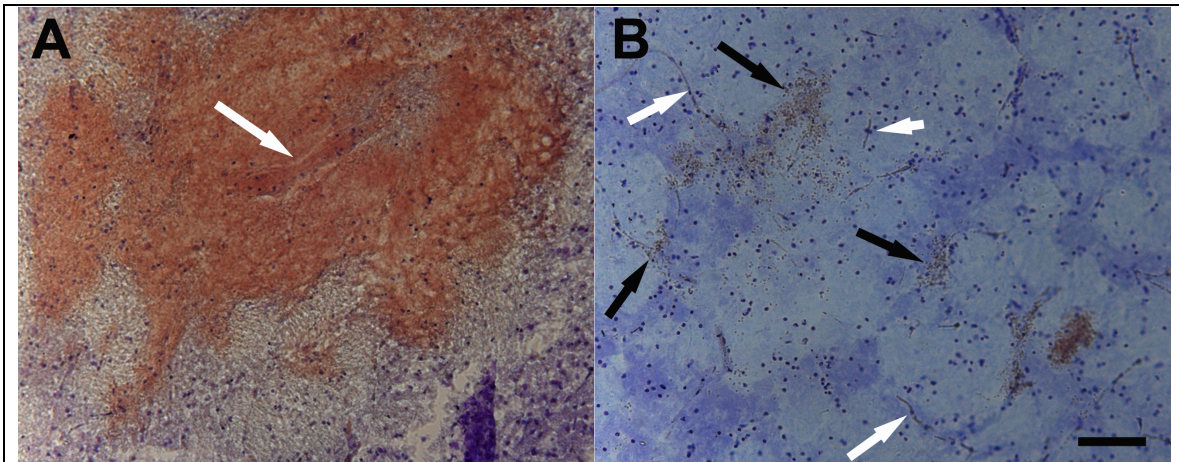
Figure 12. Appearance of different types of hemorrhage on Cresyl-violet-stained sections. Macroscopic hemorrhage (**A**), which was defined as bleeding visible to the naked eye, is shown with a bleeding vessel (arrow) in the field. Microscopic hemorrhage (**B**) with extravasated erythrocytes (black arrows) can be seen as well as obstructed vessels (white arrows). Scale bar = 100µm

Such regions usually showed co-location of extravascular red blood cells in the structurally preserved brain tissue with or without obstruction of cerebral microvessels with red blood cells, as well as formation of small blood clots by the extravasated blood.

3.7 Image Analysis: Extravasation of Evans Blue

Fluoroscopy images served to identify the Evans blue marker on all sections. Images were examined on a standard fluorescent microscope using a Nikon CY3 filter set and captured with a digital microscope camera AxioCam IC (Carl Zeiss AG, Germany). Strong and weak appearance of Evans blue were distinguished by identifying regions where more than 50% or less than 50% of visible cells had taken up the marker (Figure 13).

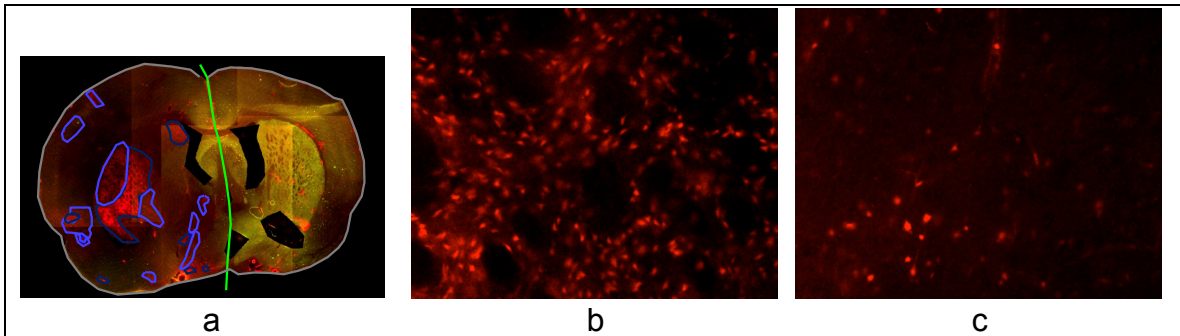**Figure 13: Fluorescence microscopy of extravasated Evan's Blue** (a). Under 20x magnification, regions of strong permeability (dark blue, b) and regions of weaker permeability (light blue, c) can be identified.

3.8 Alignment of In-Vivo Imaging and Histology

For all histology sections, overview images showing the whole brain were generated via an in-house Matlab application (The MathWorks, Inc., Natick, MA) that allows stitching of multiple low-power images. All ROIs identified directly on the microscope (infarction, macroscopic and microscopic hemorrhage, strong and weak extravasation of Evans blue) were transferred onto the overview images using Matlab.

The in-vivo and histology images were obtained almost simultaneously, approximately 30 min apart. However, in order to address a possible evolution in the degree of hemispheric brain swelling, and deformation of the specimen occurring during the histology processing, in-vivo and histology image data were co-registered based on an anatomical atlas of the rat brain (George Paxinos 2005). Eighteen distinct slices from this atlas were selected that axially covered all imaged brain regions. A set of 20 landmarks was chosen, visible on histology sections and the T2-weighted MRI images. A multi-step elastic registration process was designed and implemented so that individual brain hemispheres and manually defined ROIs on all slices were aligned to their corresponding atlas slices. ROIs defined on ground truth microscopy slides were made available on the in-vivo permeability and perfusion maps (Figure 14).
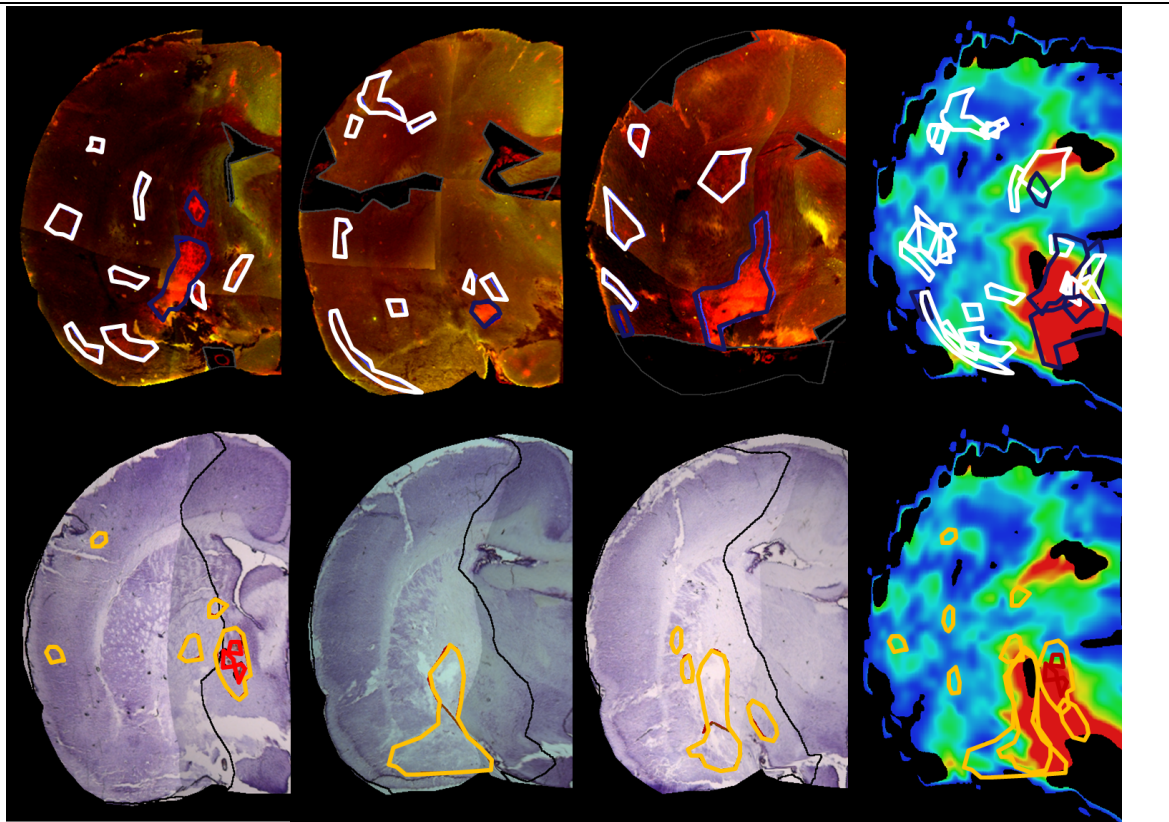
Figure 14: Blood-brain barrier disruption observed by Patlak permeability measurements on a 2mm-thick MR slice in a representative animal and corresponding histological slides. The first row shows three consecutive Evans blue slices, the second row shows three consecutive Cresyl Violet stained sections, which are matched to one MRI slice with permeability measurements. Evans blue and MRI slices, as well as Cresyl Violet and MRI slices, were individually aligned to the atlas, allowing for the transfer of ROIs, identified on histology, to the corresponding MRI slice for permeability measurements (strong permeability - blue, weak permeability - white, infarction - black, macroscopic hemorrhage - red, microscopic hemorrhage - yellow). Evans blue extravasation overlap partially with regions of hemorrhagic transformation. Both occurred mainly in the striatal area.

Once registration was completed, permeability values in the ROIs delineating the infarction and hemorrhages (macroscopic and microscopic) were recorded. CBF, CBV and MTT values within these ROIs were also recorded. CBF, CBV, MTT and permeability values were also recorded in the contralateral, nonischemic hemisphere.

To assess the accuracy of the registration process, the position of visible anatomical structures was marked separately and in a blinded fashion on selected Cresyl-violet sections and on the atlas. The average distance between

the location of these structures on the Cresyl-violet sections and their location on the atlas, used as a reference, was calculated.

3.9 Statistical analysis

Permeability values in the macroscopic and microscopic hemorrhagic ROIs were compared to the strong and weak Evans blue ROIs using a linear mixed regression model to values in the contralateral, nonischemic hemisphere or values in the infarcted hemisphere, but outside the drawn ROIs. The linear mixed regression model approach properly reflects the structure of repeated data and takes correlations of multiple measurements per individual rat into account. Marginal means for the different ROIs were reported with standard errors (±SE). Non-parametric two-sided Mann-Whitney U tests were used to compare quantitative data between SHR and Wistar rat groups. Quantitative data was described using average, standard deviation (SD) and range. A p-value less than 0.05 was considered statistically significant for all statistical analyses.

Receiver-Operating Characteristic Analysis:

To determine the predictive value of permeability measurements for hemorrhagic transformation in ischemic stroke, receiver-operating characteristic (ROC) analysis was performed. As an extension to existing work in this area (Neumann-Haefelin et al. 2002; Ding et al. 2005; Kassner et al. 2005; Lin et al. 2007), predictions based on focal permeability abnormalities were evaluated using a pixel-by-pixel thresholding approach, thereby examining the possibility to automatically predict occurrence, location and extent of HT from in-vivo imaging. The ROC analysis varied the threshold to identify focal lesions of abnormally high permeability. This analysis included all imaging slices.

The analysis was performed once for all brain voxels of the ipsilateral side to the infarct and then for only brain voxels in the infarcted brain regions. For this analysis, voxels were automatically classified into exhibiting increased permeability, hence belonging to a focal permeability abnormality, or not belonging to a focal permeability abnormality.

Previous works used manually defined focal permeability lesions (Kassner et al. 2005; Lin et al. 2007), or automated detection either through an increase of permeability over the contralateral hemisphere by more than two standard deviations (Neumann-Haefelin et al. 2002; Ding et al. 2006), or through an absolute threshold (Hom et al. 2011). We normalized our Patlak-based permeability maps to a target median CBV of 3 ml 100g^{-1} min^{-1} on the contralateral hemisphere, which allowed for the use of fixed thresholds. A range of such thresholds was applied according to the receiver operating characteristic analysis.

After thresholding, the resulting mask images were morphologically processed with an open-close operation (using a cross in a 3x3 matrix as structuring element) to generate masks that contain coherent focal permeability abnormalities on a clean background. This classification was compared to ground truth obtained from histology. Subsequently, histology slices and permeability maps were co-registered using the semi-automatic method described above. Histology findings, identified directly at the microscope (macroscopic and microscopic hemorrhage) were transferred onto computer images for each slice. Thereafter, manually defined anatomical landmarks served to guide an elastic registration of both, permeability maps and histology slices with their ground truth ROIs to a rat brain atlas (George Paxinos 2005). In these co-registered slices (Figure 15), all pixels in the ipsilateral hemisphere or the infarcted area are automatically identified as true negative, true positive, false positive, or false negative, with respect to the prediction by thresholding the permeability maps and the ground truth from histology. The precision of the elastic registration method was calculated as 0.34mm (see below), which is close to the size of one pixel in the permeability maps. Therefore, the identification of true positive and true negative pixels allowed for a mismatch between the outlines of ground truth ROIs and automatically identified ROIs by one pixel, but did not allow a change in the area or total number of pixels in the automatically identified ROIs.
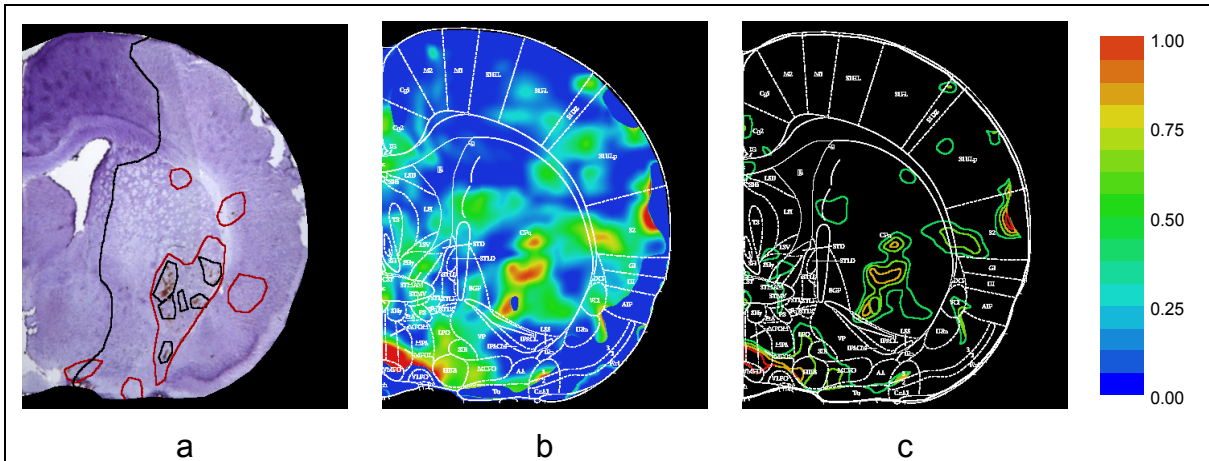
Figure 15: Co-registered slice from histology with a manually defined ROI identifying macroscopic (black) and microscopic (red) hemorrhage (a), and matching permeability map obtained 4h after reperfusion (b). Thresholding at different levels (0.4, 0.6, 0.8, 1.0 ml/min/100g) provides predictions that are then compared to the histological gold standard (c). Atlas information is overlaid for orientation.

The precision of the elastic registration method has been reported as 0.34mm (described below), which is close to the size of one pixel in the permeability maps. Therefore, the identification of true positive and true negative pixels allowed for a mismatch between the gold standard histology ROIs and automatically identified MR ROIs by one pixel, but did not allow for a change in the area or total number of pixels in the automatically identified ROIs.

The analysis was performed for all three imaging time points and comparing focal permeability abnormalities to ROIs showing macroscopic hemorrhage equal to ROIs showing macroscopic and microscopic hemorrhage on histology.

4 Results

4.1 Study population

Eleven male SHR rats and eleven male Wistar rats of 220–280 grams (Charles River laboratory) were subjected to a 2h filament occlusion of the right middle

cerebral artery. MR imaging was obtained during occlusion, as well as 4h and 24h after reperfusion. The present study focuses on the MR imaging obtained 24h after reperfusion, just before injection of Evans blue and euthanization. The MR imaging during occlusion was used to confirm the inclusion of the animals in the study. The MR imaging obtained at 4h after reperfusion served to assess the degree of reperfusion.

Animals were excluded from the study if the perfusion imaging showed no reperfusion or if the DWI lesion during occlusion involved only subcortical regions, but not the cortex. This criteria led to the exclusion of seven normal Wistar rats and 1 spontaneously hypertensive rat. In addition, 1 SHR rat was excluded, as it died shortly after reperfusion due to vessel perforation. The imaging and histological characteristics of the remaining 9 male SHR rats and 4 male Wistar rats are described in Table 3.

4.2 Infarct characteristics

The infarct size on DWI 4h after reperfusion significantly differed between SHR and Wistar rats, whereas the same final infarction pattern was obtained in both rat strains during occlusion and at 24h post reperfusion. Regarding the final infarct size on DWI, it corresponded to the extent of infarcted tissue on the Cresyl-violet sections. Infarction patterns for Wistar and SHR rats are presented in Figure 16 and show a similar distribution of the infarcted area in both groups of rats.

Figure 16: Distribution pattern of final infarction and hemorrhage patterns at 24h in Wistar (A, left) and SHR (B, right) rats. The shading represents the fraction of animals that showed infarction (top row), macroscopic hemorrhage (center row), or microscopic hemorrhage (bottom row) in the corresponding location on Cresyl-violet sections (absent in all animals for white regions, present in all animals for black regions).

4.3 Reperfusion

Four hours after removal of the suture, reperfusion was examined on perfusion-weighted imaging (Figure 17). All animals, except two of them, showed reperfusion from 72% up to 99% (Table 3). One SHR rat did not reperfuse at all because of the coating of the occluding filament, which remained at the MCA's origin.
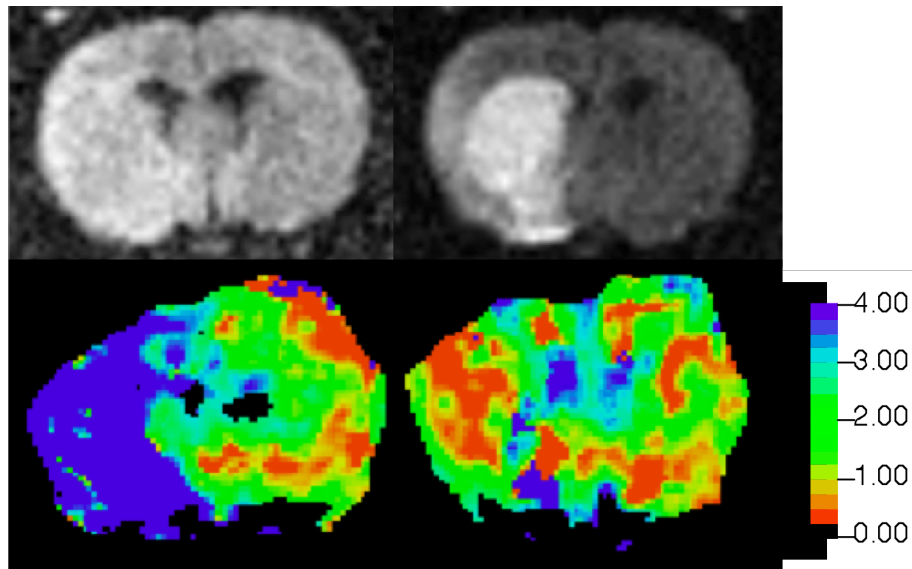
Figure 17: Occlusion and reperfusion of the right MCA territory. DWI images show a persistent hyperintensity in the right MCA territory during occlusion and 4h after reperfusion. PWI images show low perfusion in the right MCA territory during occlusion and almost complete reperfusion at 4h after removal of the filament.

4.4 Macroscopic and microscopic hemorrhage on histology

The frequency of macroscopic hemorrhage was significantly greater in SHR rats (1% of the hemisphere) compared to Wistar rats (0.1% of the hemisphere) (p = 0.02, Table 3). Microscopic hemorrhage tended to be present at 24h post reperfusion but not statistically significant between the SHR (5%) and Wistar (2%) groups (p = 0.22, Table 3).

4.5 Evans blue extravasation on histology

Strong rates of Evans blue extravasation covered 5% of the hemisphere in Wistar rats and 2% in SHR rats (p = 0.41). In contrast, weak Evans blue extravasation covered 7% of the hemisphere in Wistar rats and 3% in SHR rats (p = 0.23, Table 3).

Table 3: Volumes of DWI and PWI lesions, of infarct, of regions with abnormal permeability at 24h and at histology, and of macroscopic and microscopic hemorrhage expressed as a fraction of the total volume of the affected side.

Breed	SHR				Wistar rats				p-value
	mean	SD	min	max	mean	SD	min	max	
DWI lesion during occlusion	73%	5%	67%	77%	59%	21%	32%	78%	0.83
DWI lesion 4h post reperfusion	73%	11%	53%	85%	50%	14%	40%	71%	**0.03**
DWI lesion 24h post reperfusion	79%	6%	73%	92%	80%	6%	71%	85%	0.65
infarct on Cresyl-violet	79%	3%	73%	83%	82%	8%	74%	93%	0.53
Fraction of restored normal perfusion after reperfusion compared to PWI lesion during occlusion	87%	10%	72%*	99%	95%	4%	91%	99%	0.20
Region with abnormal permeability (increased $k1$-values) @ 24h	0.05	0.05	0.00	0.12	0.05	0.08	0.00	0.17	0.70
Strong EB extravasation	0.02	0.02	0.01	0.05	0.05	0.04	0.01	0.11	0.41
Weak EB extravasation	0.03	0.02	0.002	0.05	0.07	0.05	0.01	0.13	0.23
Macroscopic hemorrhage	1%	1%	0.1%	2%	0.1%	0.1%	0.02%	0.2%	**0.02**
Microscopic hemorrhage	5%	4%	0.8%	11%	2%	2%	0.8%	4%	0.22

* One SHR rat, which did not reperfuse, was excluded from the calculation. A reperfusion of 21% occurred in one SHR rat with a major macroscopic bleed: this rat was also excluded from the calculation because it was felt that the large hemorrhage interfered with the calculation of an accurate reperfusion rate. All other SHR rats showed a reperfusion rate of 72% to 99%.

4.6 Alignment of In-Vivo Imaging and Histology

From a total of 297 observations on 33 systematically selected Cresyl-violet slices, we determined the overall accuracy of registration as 0.34±0.28mm. This corresponds to approximately 1.1 voxels on the permeability maps. Accuracy of registration was 0.13±0.14mm (≈ 0.4 voxels), 0.38±0.22mm (≈ 1.3 voxels), and 0.30±0.27mm (≈ 1 voxel) in the cortex, preoptic area and striatum respectively.

4.7 Permeability values in different types of ROIs at 24h post reperfusion

Both Wistar and SHR rats, showed an average of 5% of increased permeability values at the 24h post reperfusion scan. There was no statistical difference between the two groups (p = 0.70) (Table 3).

Permeability values were measured in the six different types of ROIs: non-ischemic, infarct side but outside the drawn ROIs, strong extravasation of Evans blue, weak extravasation of Evans blue, microscopic hemorrhage, and macroscopic hemorrhage.

Permeability values in the non-ischemic tissue ($0.15\pm0.019^{ml}/_{min\cdot100ml}$) and permeability values on the infarct side outside the regions of interest (0.18 ± 0.018 $^{ml}/_{min\cdot100ml}$) were significantly lower than permeability values in regions of Evans blue extravasation or hemorrhage. Permeability values in regions of weak Evans blue extravasation ($0.23\pm0.016^{ml}/_{min\cdot100g}$) were significantly lower than permeability values in regions of strong Evans blue extravasation ($0.29\pm0.020^{ml}/_{min\cdot100g}$) and macroscopic hemorrhage ($0.35\pm0.049^{ml}/_{min\cdot100g}$). In contrast, permeability values in regions of microscopic hemorrhage ($0.26\pm0.024^{ml}/_{min\cdot100g}$) only differed significantly from values in regions of non-ischemic tissue. As to permeability values in the non-ischemic tissue (marginal mean±SE: $0.15\pm0.019^{ml}/_{min\cdot100g}$) and permeability values on the infarct side outside the regions of interest ($0.18\pm0.18^{ml}/_{min\cdot100g}$), they were significantly lower than all permeability values in regions of Evans blue extravasation or

hemorrhage. Moreover, permeability values in regions of weak Evans blue extravasation (0.23±0.016$^{ml}/_{min \cdot 100g}$) were significantly lower than those in regions with strong Evans blue extravasation (0.29±0.020$^{ml}/_{min \cdot 100g}$) and macroscopic hemorrhage (0.35±0.049$^{ml}/_{min \cdot 100g}$). Permeability values in regions of microscopic hemorrhage (0.26±0.024$^{ml}/_{min \cdot 100g}$) only differed significantly from values on the infarct side outside the regions of interest (0.18±0.18 $^{ml}/_{min \cdot 100g}$) or values in regions of non-ischemic tissue (0.15±0.019 $^{ml}/_{min \cdot 100g}$) (Fig. 19, Table 4).

There was no considerable statistical difference between SHR and Wistar rats regarding the permeability values within the different regions of interest.
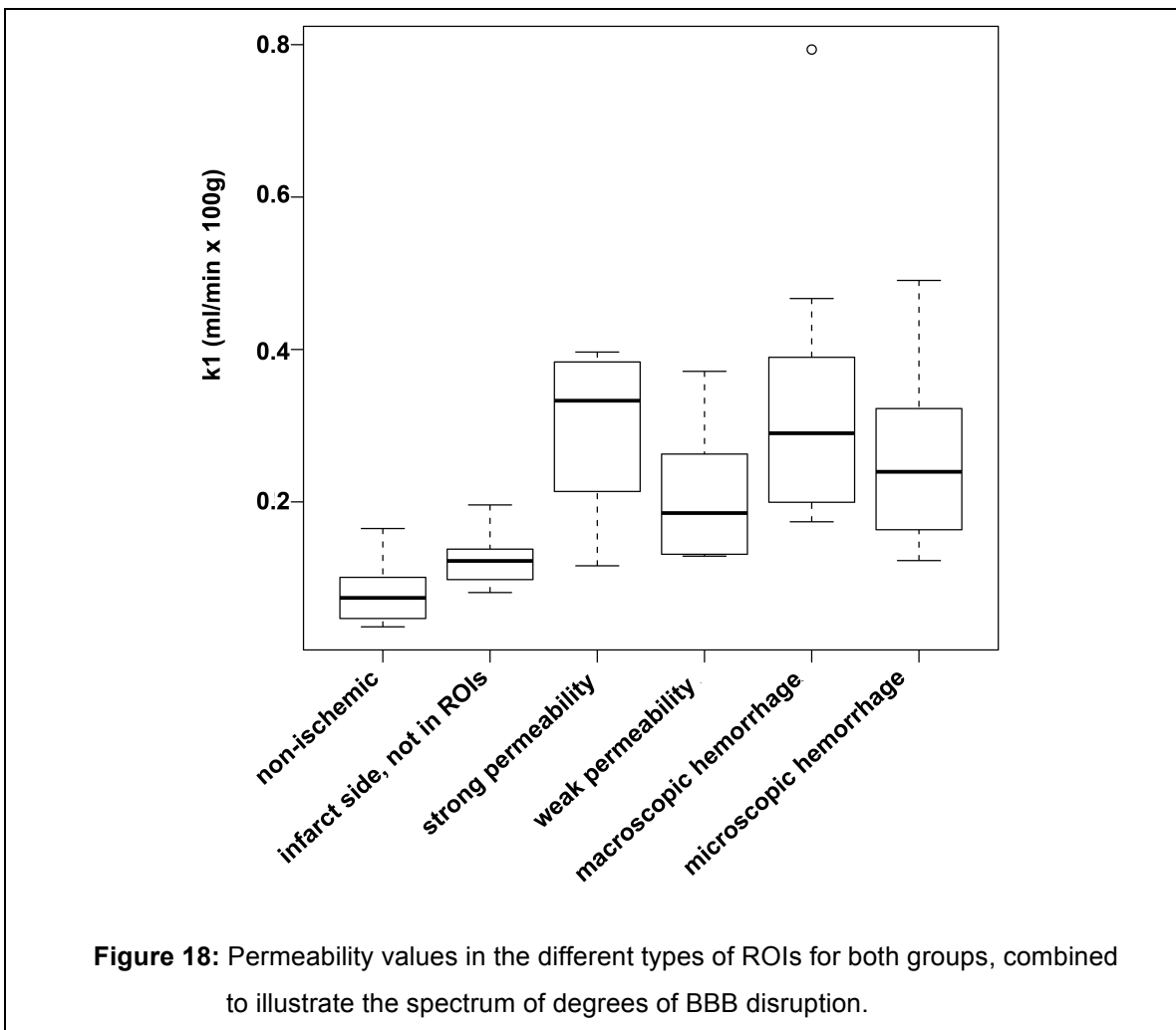

Figure 18: Permeability values in the different types of ROIs for both groups, combined to illustrate the spectrum of degrees of BBB disruption.

Table 4: Differences in estimated marginal means (± standard error) of permeability values in the different types of ROIs, which were extracted from the mixed linear regression model, are shown in the upper right triangular matrix; the corresponding p-values are displayed in the lower left triangular matrix.

Differences in estimated marginal means±SE / p-values	Non-ischemic	Strong Evans blue extravasation	Weak Evans blue extravasation	Macroscopic hemorrhage	Microscopic hemorrhage
non-ischemic	-	**-0.105±0.025**	**-0.036±0.008**	**-0.160±0.048**	**-0.070±0.020**
strong extravasation	**0.001**	-	**0.069±0.024**	-0.055±0.052	0.035±0.030
weak extravasation	**0.004**	**0.018**	-	-0.124±0.048	-0.034±0.020
macroscopic hemorrhage	**0.013**	0.317	0.038	-	0.090±0.051
microscopic hemorrhage	**0.009**	0.259	0.131	0.115	-

4.8 Receiver operating characteristic analysis

Automatically determined focal permeability abnormalities on the ipsilateral hemisphere (Figure 16) best coincided with regions of macroscopic hemorrhage when imaged 4h after reperfusion, giving an area under the ROC curve (AUC) of 83%. The ROC was similar, albeit slightly lower for predictions from imaging during occlusion (AUC 73%) or 24h after reperfusion (AUC 76%). Restricting the analysis to the infarcted area resulted in a small AUC increase in 1% at each time point, decreasing the number of false positive measurements. The ROC then showed AUC of 74%, 84% and 75% during occlusion, 4h post reperfusion and 24h post reperfusion, respectively (Figure 19). Focal permeability abnormalities were a better match to areas that showed only macroscopic hemorrhage. For comparisons to regions with both macroscopic and microscopic hemorrhage on histology in the infarcted area, the ROC analyses showed AUC of 69%, 78%, and 72% during occlusion, 4h after reperfusion, and 24h after reperfusion respectively.

Overall, the negative predictive value of BBB permeability measurements was significant, while the positive predictive value was limited. For instance, a BBB permeability threshold of 0.35 $^{ml}/_{min \cdot 100ml}$ positive and negative predictive values for imaging during occlusion were 9.5% and 96.2%, respectively. For imaging 4h post reperfusion resulted in values of 14.9% and 98.3%.

Figure 19: ROC to predict macroscopic hemorrhage on histology from blood-brain barrier permeability imaging measurements. Curves refer to imaging during perfusion (blue line), 4h after reperfusion (orange line), and 24h post reperfusion (green line).

Table 5: False (FPR) and true positive rates (TPR), positive (PPV) and negative predictive values (NPV) for automatically determined focal lesions of increased permeability 4h after reperfusion in comparison to macroscopic hemorrhage on histology. Values are presented for a wide range of permeability thresholds.

Threshold (ml/min/100g)	FPR	TPR	PPV	NPV
0.005	83%	99%	4.0%	99.7%
0.01	79%	98%	4.2%	99.7%
0.015	76%	98%	4.4%	99.7%
0.02	73%	98%	4.5%	99.7%
0.03	68%	98%	4.8%	99.7%
0.04	64%	97%	5.1%	99.7%
0.05	60%	97%	5.4%	99.7%
0.075	51%	95%	6.1%	99.5%
0.1	44%	93%	6.9%	99.5%
0.125	38%	91%	7.7%	99.3%
0.15	33%	82%	8.5%	99.1%
0.175	28%	80%	9.3%	99.1%
0.2	25%	80%	10.3%	99.0%
0.225	21%	77%	11.3%	99.0%
0.25	19%	74%	12.3%	99.0%
0.3	15%	66%	13.8%	98.6%
0.35	11%	57%	14.9%	98.3%
0.4	9%	48%	15.4%	98.0%
0.5	6%	32%	15.0%	97.5%
0.6	4%	19%	13.4%	97.1%
0.7	3%	13%	12.4%	97.0%
0.8	2%	10%	12.7%	96.9%
0.9	2%	8%	14.2%	96.8%

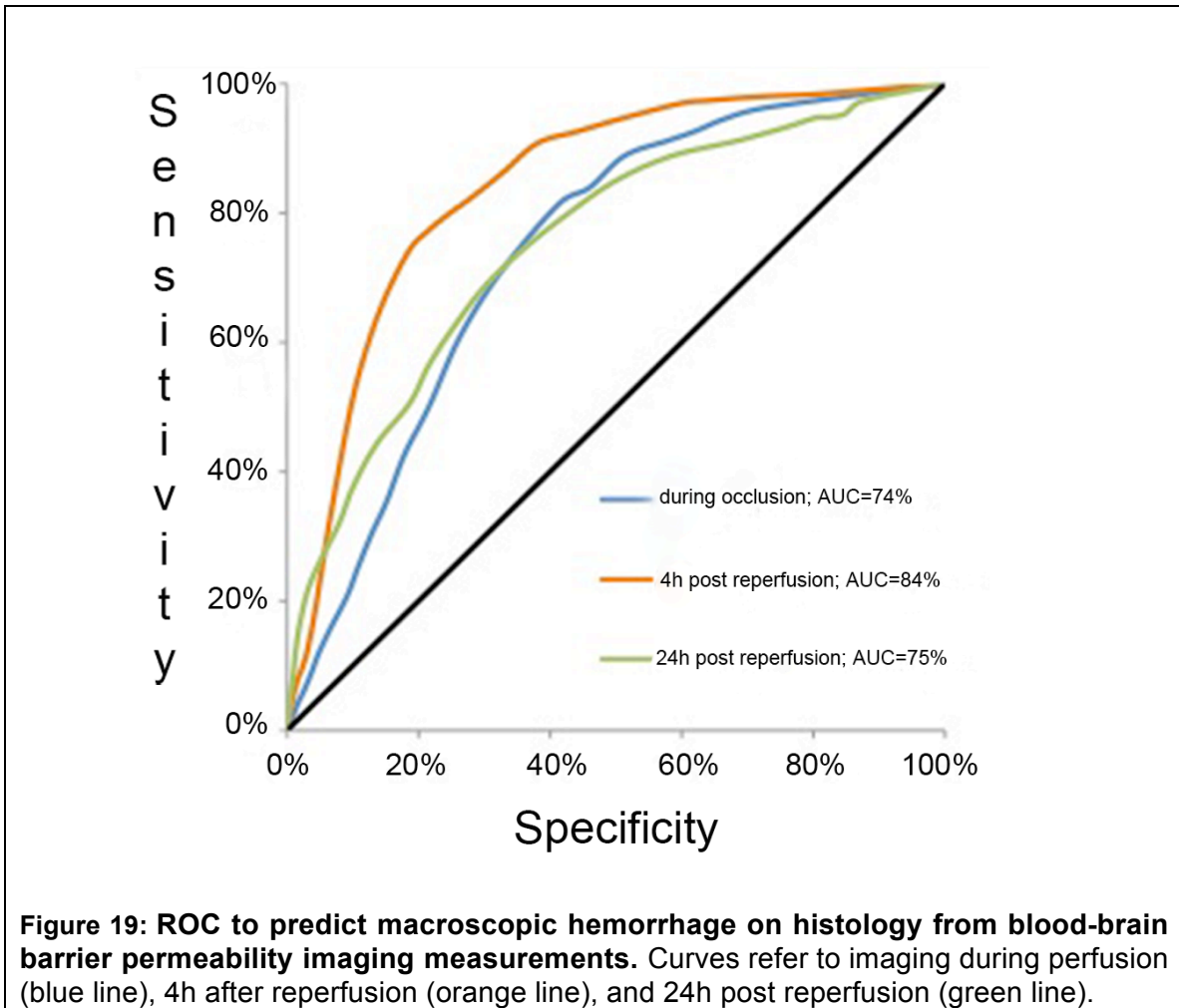|				
1	1%	7%	15.6%	96.8%
1.2	1%	4%	17.3%	96.7%
1.4	0.3%	3%	21.6%	96.7%
1.6	0.2%	2%	26.2%	96.7%
1.8	0.1%	1%	33.3%	96.6%
2	0	1%	50%	96.6%

Table 6: False (FPR) and true positive rates (TPR), positive (PPV) and negative predictive values (NPV) for automatically determined focal lesions of increased permeability during occlusion in comparison to macroscopic hemorrhage on histology. Values are presented for a wide range of permeability thresholds.

Threshold (ml/min/100g)	FPR	TPR	PPV	NPV
0.005	72%	96%	5.3%	99.4%
0.01	66%	95%	5.7%	99.3%
0.015	62%	93%	6.0%	99.2%
0.02	58%	91%	6.3%	99.1%
0.03	51%	89%	6.9%	99.0%
0.04	46%	84%	7.2%	98.7%
0.05	41%	81%	7.7%	98.7%
0.075	33%	71%	8.5%	98.2%
0.1	26%	61%	9.0%	97.8%
0.125	22%	50%	9.0%	97.4%
0.15	18%	43%	9.2%	97.1%
0.175	15%	35%	9.0%	96.9%
0.2	13%	30%	9.1%	96.7%
0.225	11%	25%	9.0%	96.6%
0.25	9%	21%	8.8%	96.4%
0.3	7%	16%	9.2%	96.3%

0.35	5%	12%	9.5%	96.2%
0.4	4%	9%	9.3%	96.1%
0.5	3%	6%	9.5%	96.1%
0.6	2%	4%	9.3%	96.0%
0.7	1%	3%	9.8%	96.0%
0.8	1%	3%	9.5%	96.0%
0.9	1%	2%	10.6%	96.0%
1	1%	2%	9.1%	96.0%
1.2	0.3%	0.8%	8.5%	96.0%
1.4	0.2%	0.4%	8.2%	96.0%
1.6	0.1%	0.2%	6.2%	96.0%
1.8	0.1%	0.2%	8.7%	96.0%
2	0	0.1%	8.3%	96.0%

5 Discussion

The purpose of the study was to first validate in-vivo BBB permeability measurements extracted from perfusion-weighted MRI by the same method used in acute stroke patients (Dankbaar et al. 2008; Dankbaar et al. 2009; Hom et al. 2009) by comparison with gold standard histology. This software relies on the Patlak model for calculating BBB permeability values, and has been previously employed in order to predict clinically significant hemorrhagic transformation in acute stroke patients receiving tPA (Hom et al. 2011).

Our results indicate that all areas of BBB disruption (Evans blue extravasation and hemorrhages) identified on gold standard histology have significantly increased permeability on MR imaging compared to non-affected brain. Remarkably, permeability imaging also allows for grading the degree of BBB disruption, as regions with strong Evans blue extravasation show higher permeability on MRI than regions with weak Evans blue extravasation on histological sections.

Regarding the validation of the BBB permeability measurements, we focused on the 24h post reperfusion time point. At 24h post reperfusion, histological signs of an ischemic injury have emerged, the endothelium is severely damaged and BBB disruption has occurred. This cross-sectional part of the study, comparing imaging and histology obtained almost simultaneously at 24h, does not allow inferences in the causal relationship between increased BBB permeability and hemorrhagic transformation in acute ischemic stroke.

In order to validate BBB as a potential indicator of hemorrhagic transformation, it is important to include observations with intact BBB values together with a wide range of permeable and disrupted BBB values to show that the pathology can be accurately detected. The hemispheric stroke model selected for this study reliably induced ischemic stroke with a diffusion lesion that affected 79% of the selected hemisphere in SHR rats and 80% in Wistar rats. SHR rats were more likely to develop macroscopic hemorrhage compared to Wistar rats, which is in agreement with previously performed studies (Asahi et al. 2000; Neumann-

Haefelin et al. 2002; Ding et al. 2005). However, the permeability values were not significantly different in SHR and Wistar rats, which might be caused by the small sample size. Further investigation will be necessary to address this issue.

Additionally, in order to minimize the observer-expectancy effect we introduced a landmark-orientated registration approach. MR images as well as histological sections were co-registered to an anatomical atlas of the rat brain, which allowed spot-on matching of MR images and histological sections. This method may be more reliable than hand-drawn ROIs used in various other validation studies.

In this study, we measured quantitative BBB permeability values applying the same modified Patlak model currently used in patients (Hom et al. 2011). In this modified model (Schneider et al. 2011), one stabilization step was added to the original Patlak model, which had been successfully applied to dynamic contrast-enhanced MRI data to quantify BBB permeability after middle cerebral artery occlusion in rats (Ewing et al. 2003; Knight et al. 2005).

While the above study shows the sensitivity of in-vivo BBB measurements by imaging, it also identifies limitations:

Imaging assessment of the BBB permeability cannot distinguish between different causes for contrast agent extravasation, namely permeation through an open BBB in otherwise intact vasculature and leakage of contrast agent through damaged vascular walls.

An additional limitation of this study is that Gd-DTPA (molecular weight 552 Da) and Evans blue tagged albumin (~68kDa) vary in size and distribution volumes. Different extravasation mechanisms for both agents are also described *in vitro* and *in vivo* under conditions of hypoxia (Plateel et al. 1997; Sood et al. 2009). However, a reperfusion injury after 2h middle cerebral artery occlusion produces extensive damage to the whole neurovascular unit including tight junctions and endothelial cells. Therefore, even if the amount of extravasated Gd-DTPA and Evans blue tagged albumin may be different due to their respective sizes, the

locations of Evans blue leakage on histology and areas with increased permeability values on Gd-DTPA imaging were the same, and as such the comparison is justified.

Gd-DTPA can be linked to bovine serum albumine (BSA) and Evans blue; it then has similar properties and a similar extravasation mechanism to Evans blue. Gd-BSA-EB has been studied in the setting of BBBP in ischemic stroke (Nagaraja et al. 2008), but was not applied in this study in order to utilize the same imaging method already used in patients.

Subsequent to our validation, that regions of increased permeability measured in vivo by imaging coincide with BBB disruption and hemorrhage observed on gold standard histology, we evaluated the predictive value of these measurements in terms of hemorrhagic transformation.

Not all hemorrhagic infarction types lead to clinical deterioration (Molina et al. 2002); symptomatic hemorrhagic transformation is associated with worse clinical outcome (Fiorelli et al. 1999) and has been related to severe hypoperfusion and aggressive treatment (Kim et al. 2010). Reducing the incidence of symptomatic hemorrhage with extended reperfusion therapy remains a great challenge. In the course of ongoing efforts to extend the time window, risk assessment of hemorrhagic transformation in individual patients would provide valuable information.

In extension to previous work by other research groups, we used automatically detected focal BBBP lesions to predict occurrence, location, and size of areas affected by HT. The prediction analysis, using a pixel-by-pixel thresholding approach paired with a ROC analysis for different threshold decisions on permeability maps, showed significant negative predictive value, while the positive predictive value was limited. Those findings illustrate that increased BBB permeability on imaging is specific in detecting lesions with increased permeability; however, increased permeability does not necessarily lead to hemorrhagic transformation. Thus, altered BBBP is present at locations of

47

hemorrhagic transformation in rats with an infarct, but further risk factors need to be considered in combination with BBBP to reliably predict hemorrhagic transformation.

The performed ROC analysis showed a similar predictive power in terms of hemorrhagic transformation for all three time points (occlusion, 4h post reperfusion and 24h post reperfusion), with better prediction at 4h post reperfusion, and overall slightly better prediction if the ROC analysis was restricted to the infarct area. This suggests that the role of an altered blood-brain barrier permeability in the occurrence of hemorrhagic transformation in a rat model of 2h transient MCA occlusion remains relatively constant over time, with a mild increase shortly after reperfusion.

Reperfusion after an ischemic event triggers several molecular mechanisms and can increase the risk of hemorrhagic transformation (Wang and Lo 2003; Kim et al. 2010), which might explain higher BBBP values after reperfusion than during occlusion. Furthermore, reperfusion accrues oxidative stress, causing damage to lipid-rich membranes in the BBB and leading to vascular leakage (Chan 1994; Gursoy-Ozdemir et al. 2004). Neuroinflammatory mechanisms, alterations in cytokine profiles, adhesion-molecule expression and tight junction components equally contribute to vascular leakage after reperfusion (Wang and Lo 2003). Another explanation for the increased BBBP values after reperfusion could be that higher amounts of contrast agent reaching the infarcted territory lead to a higher detection on MR imaging.

In terms of hemorrhage type, the performed ROC analysis showed better predictive power for macroscopic hemorrhage only than for macroscopic and microscopic hemorrhage combined. This suggests that increased BBB permeability occurs more often in regions of macroscopic hemorrhage. Moreover, hemorrhagic transformation mainly occurred in infarct area, being the area most at risk for this complication.

The potential of BBBP imaging for predicting hemorrhagic transformation in rodent models of stroke (Knight et al. 1998; Jiang et al. 2002; Neumann-Haefelin et al. 2002) has been investigated and was first shown using post-contrast T1-weighted MRI (Knight et al. 1998). Later studies quantified BBB disruption using dynamic contrast enhanced imaging in order to predict subsequent hemorrhage. Dynamic contrast enhanced imaging detected microscopic and macroscopic hemorrhage in a model of embolic stroke treated with rtPA and a neuroprotective agent; however, no distinction could be drawn between the hemorrhage subtypes (Ding et al. 2006).

Several studies have evaluated the role of BBBP imaging in stroke patients and showed that HT types vary when BBB disruption is present and that several diagnostic and therapeutic factors are independently associated with HT, including elevated glucose levels and diastolic pressure (Bang et al. 2009; Kassner et al. 2009). BBBP imaging using CT showed abnormal BBBP to have a high sensitivity and specificity if combined with older age and rtPA (Hom et al. 2011).

BBBP is a promising imaging tool for obtaining information with regard to microvascular status. However, by itself, BBBP imaging might not be specific enough to predict symptomatic hemorrhagic transformation. Meanwhile, identifying further risk factors and combining them with a BBBP threshold might increase the sensitivity to predict symptomatic HT in acute stroke and value for HT risk assessment. Further research will be necessary to find a reliable combination of BBBP threshold and additional risk factors. Adding BBBP information to existing clinical risk scores, such as the hemorrhage after thrombolysis (HAT) or Multicenter Stroke survey (MSS) scores, might increase the sensitivity to predict symptomatic HT.

Basic and clinical studies can both contribute to this goal. Nevertheless, it is important to remember that a transient MCA occlusion model in the experimental setup represents but one specific type of ischemic stroke with controlled, timed reperfusion and low intergroup variance, and is not necessarily comparable to

ischemic stroke in patients. Furthermore, differences between rodents and humans in terms of vascular anatomy and physiology should be kept in mind. Primates and patients possess a more complex collateral protection than rodents (Fukuda and del Zoppo 2003). Higher collateral flow during occlusion might explain why higher cerebral blood flow and volume are measured in the infarcted tissue in humans, and why higher blood-brain barrier permeability values can be recorded during occlusion in humans versus rats. In this study, we have focused on a BBBP pixel-by-pixel approach in order to find a threshold to predict hemorrhagic transformation. However, adding additional variables such as vascular density or collateral flow might add valuable information and will be addressed in further experimental and clinical studies.

In conclusion, our study indicates that BBBP measurements help to predict the subsequent risk of hemorrhagic transformation. Further research, however, is required to identify the additional risk factors that need to be present; and thus in combination with an increased blood-brain barrier permeability, to create a reliable method for risk assessment in hemorrhagic transformation in the setting of stroke.

6 Summary

Symptomatic hemorrhagic transformation is associated with worse clinical outcome in acute ischemic stroke. Reducing the incidence of symptomatic hemorrhage with extended reperfusion therapy remains a great challenge. With the ongoing efforts to extent the time window, risk assessment of hemorrhagic transformation in each patient would add valuable information. Increased blood-brain barrier permeability has pathophysiologically been associated with hemorrhagic transformation.

The scope of this MD thesis was to obtain blood-brain barrier permeability measurements extracted from contrast-enhanced MRI through a relatively simple and frequently applied model, the Patlak model, and to validate them against gold standard histology in an adult rat model of ischemic stroke. Blood–brain barrier permeability (BBBP) was shown on histology by the extravasation of Evans blue on fluorescence microscopy sections matching location and orientation of MR images. Cresyl-violet staining served to identify and characterize hemorrhage. Automatically detected focal blood-brain barrier permeability lesions were used to predict occurrence, location, and extent of hemorrhagic transformation. Receiver-operating characteristic analysis paired with a pixel-by-pixel approach was performed to determine the most accurate BBBP threshold.

Regions of increased permeability measured in-vivo by MR imaging, using the same method already applied in patients, coincided with blood-brain barrier disruption and hemorrhage observed on gold standard histology. The prediction analysis showed a significant negative predictive value, while the positive predictive value was limited.

In conclusion, altered blood-brain barrier permeability is present at locations of hemorrhagic transformation in rats with an infarct, but further risk factors need to be considered in combination with blood-brain barrier permeability to reliably predict hemorrhagic transformation.

5   Zusammenfassung

Symptomatische hämorrhagische Transformation (HT) nach akutem ischämischen Schlaganfall geht mit einem schlechteren klinischen Verlauf einher. Es bleibt eine große Herausforderung, die Inzidenz der symptomatischen HT im Rahmen von erweiterten Reperfusiontherapien zu reduzieren. Zur Unterstützung fortschreitender Bemühungen um eine Erweiterung des Thrombloysezeitfensters würden patientenindividuelle Risikoanalysen zur HT nützliche Aussagen liefern. Erhöhte Permeabilität der Blut-Hirn-Schranke wird mit HT in Verbindung gesetzt.

In dieser Doktorarbeit wurden an einem ischämischen Schlaganfallmodell der Ratte Messungen zur Permeabilität der Blut-Hirn-Schranke in der Kontrast-verstärkten MRT durchgeführt. Die Auswertung erfolgte mit dem Patlak-Modell. Dieses verhältnismäßig einfache und häufig angewandte Modell wurde auf Gültigkeit gegenüber der Goldstandard Histologie überprüft. Die Durchlässigkeit der Blut-Hirn-Schranke wurde auf histologischen Schnitten durch Austritt von Evans blue mittels Fluoreszensmikroskopie bestätigt und den entsprechenden MR Bildern zugeordnet. Blutungen wurden anhand von Cresyl-Violet Färbung identifiziert und charakterisiert. Um Häufigkeit, Lage und Größe der von hämorrhagischer Transformation betroffenen Regionen vorauszusagen, wurde ein Schwellwertverfahren verwendet, das automatisch fokale Läsionen erhöhter Permeabilität ermittelt. Die durchgeführte Prädiktionsanalyse erfolgte individuell für jeden Bildpunkt, kombiniert mit einer ROC Analyse für unterschiedliche Schwellwerte. Mithilfe dieser zuvor bereits an Patienten angewandten Methode gelang es zu zeigen, dass in der MRT gemessene Regionen erhöhter Permeabilität mit Blut-Hirn-Schranken-Störung und Blutung in der Histologie übereinstimmen. Die durchgeführte Prädiktionsanalyse zeigte einen signifikant negativen prädiktiven Wert, während der positive prädiktive Wert eingeschränkte Aussagekraft hatte.

Als Endergebnis lässt sich festhalten, dass Ratten mit Schlaganfall eine erhöhte Permeabilität der Blut-Hirn-Schranke an Stellen von sich entwickelnder HT aufweisen. Allerdings gilt es weitere Risikofaktoren in Kombination mit Permeabilität zu prüfen, um hämorrhagische Transformation verlässlich vorherzusagen.

7 References

ADAMS, H. P., JR., B. H. BENDIXEN, L. J. KAPPELLE, J. BILLER, B. B. LOVE, D. L. GORDON and E. E. MARSH, 3RD (1993): Classification of subtype of acute ischemic stroke. Definitions for use in a multicenter clinical trial. TOAST. Trial of Org 10172 in Acute Stroke Treatment. *Stroke* 24, 35-41.

ADAMS, H. P., JR., G. DEL ZOPPO, M. J. ALBERTS, D. L. BHATT, L. BRASS, A. FURLAN, R. L. GRUBB, R. T. HIGASHIDA, E. C. JAUCH, C. KIDWELL, P. D. LYDEN, L. B. MORGENSTERN, A. I. QURESHI, R. H. ROSENWASSER, P. A. SCOTT and E. F. WIJDICKS (2007): Guidelines for the early management of adults with ischemic stroke: a guideline from the American Heart Association/American Stroke Association Stroke Council, Clinical Cardiology Council, Cardiovascular Radiology and Intervention Council, and the Atherosclerotic Peripheral Vascular Disease and Quality of Care Outcomes in Research Interdisciplinary Working Groups: the American Academy of Neurology affirms the value of this guideline as an educational tool for neurologists. *Stroke* 38, 1655-1711.

ALBERS, G. W., V. N. THIJS, L. WECHSLER, S. KEMP, G. SCHLAUG, E. SKALABRIN, R. BAMMER, W. KAKUDA, M. G. LANSBERG, A. SHUAIB, W. COPLIN, S. HAMILTON, M. MOSELEY and M. P. MARKS (2006): Magnetic resonance imaging profiles predict clinical response to early reperfusion: the diffusion and perfusion imaging evaluation for understanding stroke evolution (DEFUSE) study. *Ann Neurol* 60, 508-517.

ALFKE, K., U. JENSEN, C. POOL, A. ROHR, R. BRUNING, J. WEBER, T. BARTSCH, R. STINGELE and O. JANSEN (2011): Contrast-enhanced magnetic resonance angiography in stroke diagnostics: additional information compared with time-of-flight magnetic resonance angiography? *Clin Neuroradiol* 21, 5-10.

ASAHI, M., K. ASAHI, X. WANG and E. H. LO (2000): Reduction of tissue plasminogen activator-induced hemorrhage and brain injury by free radical spin trapping after embolic focal cerebral ischemia in rats. *J Cereb Blood Flow Metab* 20, 452-457.

AVIV, R. I., C. D. D'ESTERRE, B. D. MURPHY, J. J. HOPYAN, B. BUCK, G. MALLIA, V. LI, L. ZHANG, S. P. SYMONS and T. Y. LEE (2009): Hemorrhagic transformation of ischemic stroke: prediction with CT perfusion. *Radiology* 250, 867-877.

AXEL, L. (1983): Tissue mean transit time from dynamic computed tomography by a simple deconvolution technique. *Invest Radiol* 18, 94-99.

Bang, O. Y., B. H. Buck, J. L. Saver, J. R. Alger, S. R. Yoon, S. Starkman, B. Ovbiagele, D. Kim, L. K. Ali, N. Sanossian, R. Jahan, G. R. Duckwiler, F. Vinuela, N. Salamon, J. P. Villablanca and D. S. Liebeskind (2007): Prediction of hemorrhagic transformation after recanalization therapy using T2*-permeability magnetic resonance imaging. *Ann Neurol* 62, 170-176.

Bang, O. Y., J. L. Saver, J. R. Alger, S. H. Shah, B. H. Buck, S. Starkman, B. Ovbiagele and D. S. Liebeskind (2009): Patterns and predictors of blood-brain barrier permeability derangements in acute ischemic stroke. *Stroke* 40, 454-461.

Bash, S., J. P. Villablanca, R. Jahan, G. Duckwiler, M. Tillis, C. Kidwell, J. Saver and J. Sayre (2005): Intracranial vascular stenosis and occlusive disease: evaluation with CT angiography, MR angiography, and digital subtraction angiography. *AJNR Am J Neuroradiol* 26, 1012-1021.

Belayev, L., R. Busto, W. Zhao and M. D. Ginsberg (1996): Quantitative evaluation of blood-brain barrier permeability following middle cerebral artery occlusion in rats. *Brain Res* 739, 88-96.

Berger, C., M. Fiorelli, T. Steiner, W. R. Schabitz, L. Bozzao, E. Bluhmki, W. Hacke and R. von Kummer (2001): Hemorrhagic transformation of ischemic brain tissue: asymptomatic or symptomatic? *Stroke* 32, 1330-1335.

Bisdas, S., M. Hartel, L. H. Cheong and T. S. Koh (2007): Detection of early vessel leakiness in acute ischemic stroke using computed tomography perfusion may indicate hemorrhagic transformation. *Acta Radiol* 48, 341-344.

Broderick, J. P. and IMS (2007): The Interventional Management of Stroke (IMS) II Study. *Stroke* 38, 2127-2135.

Burggraf, D., A. Trinkl, J. Burk, H. K. Martens, M. Dichgans and G. F. Hamann (2008): Vascular integrin immunoreactivity is selectively lost on capillaries during rat focal cerebral ischemia and reperfusion. *Brain Res* 1189, 189-197.

Chalela, J. A., C. S. Kidwell, L. M. Nentwich, M. Luby, J. A. Butman, A. M. Demchuk, M. D. Hill, N. Patronas, L. Latour and S. Warach (2007): Magnetic resonance imaging and computed tomography in emergency assessment of patients with suspected acute stroke: a prospective comparison. *Lancet* 369, 293-298.

CHAN, P. H. (1994): Oxygen radicals in focal cerebral ischemia. *Brain Pathol* 4, 59-65.

CHRISTENSEN, S., K. MOURIDSEN, O. WU, N. HJORT, H. KARSTOFT, G. THOMALLA, J. ROTHER, J. FIEHLER, T. KUCINSKI and L. OSTERGAARD (2009): Comparison of 10 perfusion MRI parameters in 97 sub-6-hour stroke patients using voxel-based receiver operating characteristics analysis. *Stroke* 40, 2055-2061.

CLARK, W. M., S. WISSMAN, G. W. ALBERS, J. H. JHAMANDAS, K. P. MADDEN and S. HAMILTON (1999): Recombinant tissue-type plasminogen activator (Alteplase) for ischemic stroke 3 to 5 hours after symptom onset. The ATLANTIS Study: a randomized controlled trial. Alteplase Thrombolysis for Acute Noninterventional Therapy in Ischemic Stroke. *JAMA* 282, 2019-2026.

DANI, K. A., R. G. THOMAS, F. M. CHAPPELL, K. SHULER, M. J. MACLEOD, K. W. MUIR and J. M. WARDLAW (2011): Computed tomography and magnetic resonance perfusion imaging in ischemic stroke: definitions and thresholds. *Ann Neurol* 70, 384-401.

DANKBAAR, J. W., J. HOM, T. SCHNEIDER, S. C. CHENG, B. C. LAU, I. VAN DER SCHAAF, S. VIRMANI, S. POHLMAN, W. P. DILLON and M. WINTERMARK (2008): Accuracy and anatomical coverage of perfusion CT assessment of the blood-brain barrier permeability: one bolus versus two boluses. *Cerebrovasc Dis* 26, 600-605.

DANKBAAR, J. W., J. HOM, T. SCHNEIDER, S. C. CHENG, B. C. LAU, I. VAN DER SCHAAF, S. VIRMANI, S. POHLMAN, W. P. DILLON and M. WINTERMARK (2008): Dynamic perfusion CT assessment of the blood-brain barrier permeability: first pass versus delayed acquisition. *AJNR Am J Neuroradiol* 29, 1671-1676.

DANKBAAR, J. W., J. HOM, T. SCHNEIDER, S. C. CHENG, B. C. LAU, I. VAN DER SCHAAF, S. VIRMANI, S. POHLMAN and M. WINTERMARK (2009): Age- and anatomy-related values of blood-brain barrier permeability measured by perfusion-CT in non-stroke patients. *J Neuroradiol* 36, 219-227.

DAVIS, S. M., G. A. DONNAN, M. W. PARSONS, C. LEVI, K. S. BUTCHER, A. PEETERS, P. A. BARBER, C. BLADIN, D. A. DE SILVA, G. BYRNES, J. B. CHALK, J. N. FINK, T. E. KIMBER, D. SCHULTZ, P. J. HAND, J. FRAYNE, G. HANKEY, K. MUIR, R. GERRATY, B. M. TRESS and P. M. DESMOND (2008): Effects of alteplase beyond 3 h after stroke in the Echoplanar Imaging Thrombolytic Evaluation Trial (EPITHET): a placebo-controlled randomised trial. *Lancet Neurol* 7, 299-309.

DEBREY, S. M., H. YU, J. K. LYNCH, K. O. LOVBLAD, V. L. WRIGHT, S. J. JANKET and A. E. BAIRD (2008): Diagnostic accuracy of magnetic resonance angiography for internal carotid artery disease: a systematic review and meta-analysis. *Stroke* 39, 2237-2248.

DIJKHUIZEN, R. M., M. ASAHI, O. WU, B. R. ROSEN and E. H. LO (2002): Rapid breakdown of microvascular barriers and subsequent hemorrhagic transformation after delayed recombinant tissue plasminogen activator treatment in a rat embolic stroke model. *Stroke* 33, 2100-2104.

DING, G., Q. JIANG, L. LI, L. ZHANG, Z. GANG ZHANG, K. A. LEDBETTER, J. R. EWING, Q. LI and M. CHOPP (2006): Detection of BBB disruption and hemorrhage by Gd-DTPA enhanced MRI after embolic stroke in rat. *Brain Res* 1114, 195-203.

DING, G., V. NAGESH, Q. JIANG, L. ZHANG, Z. G. ZHANG, L. LI, R. A. KNIGHT, Q. LI, J. R. EWING and M. CHOPP (2005): Early prediction of gross hemorrhagic transformation by noncontrast agent MRI cluster analysis after embolic stroke in rat. *Stroke* 36, 1247-1252.

EASTWOOD, J. D., M. H. LEV and J. M. PROVENZALE (2003): Perfusion CT with iodinated contrast material. *AJR Am J Roentgenol* 180, 3-12.

EWING, J. R., R. A. KNIGHT, T. N. NAGARAJA, J. S. YEE, V. NAGESH, P. A. WHITTON, L. LI and J. D. FENSTERMACHER (2003): Patlak plots of Gd-DTPA MRI data yield blood-brain transfer constants concordant with those of 14C-sucrose in areas of blood-brain opening. *Magn Reson Med* 50, 283-292.

FENSTERMACHER, J. D., R. A. KNIGHT, J. R. EWING, T. NAGARAJA, V. NAGESH, J. S. YEE and P. A. ARNIEGO (2003): Estimating blood-brain barrier opening in a rat model of hemorrhagic transformation with Patlak plots of Gd-DTPA contrast-enhanced MRI. *Acta Neurochir Suppl* 86, 35-37.

FIEBACH, J. B., P. D. SCHELLINGER, A. GASS, T. KUCINSKI, M. SIEBLER, A. VILLRINGER, P. OLKERS, J. G. HIRSCH, S. HEILAND, P. WILDE, O. JANSEN, J. ROTHER, W. HACKE and K. SARTOR (2004): Stroke magnetic resonance imaging is accurate in hyperacute intracerebral hemorrhage: a multicenter study on the validity of stroke imaging. *Stroke* 35, 502-506.

FIORELLI, M., S. BASTIANELLO, R. VON KUMMER, G. J. DEL ZOPPO, V. LARRUE, E. LESAFFRE, A. P. RINGLEB, S. LORENZANO, C. MANELFE and L. BOZZAO (1999): Hemorrhagic transformation within 36 hours of a cerebral infarct: relationships with early clinical deterioration and 3-month outcome in the European Cooperative Acute Stroke Study I (ECASS I) cohort. *Stroke* 30, 2280-2284.

FUKUDA, S. and G. J. DEL ZOPPO (2003): Models of focal cerebral ischemia in the nonhuman primate. *ILAR J* 44, 96-104.

FURLAN, A., R. HIGASHIDA, L. WECHSLER, M. GENT, H. ROWLEY, C. KASE, M. PESSIN, A. AHUJA, F. CALLAHAN, W. M. CLARK, F. SILVER and F. RIVERA (1999): Intra-arterial prourokinase for acute ischemic stroke. The PROACT II study: a randomized controlled trial. Prolyse in Acute Cerebral Thromboembolism. *JAMA* 282, 2003-2011.

FURLAN, A. J., D. EYDING, G. W. ALBERS, Y. AL-RAWI, K. R. LEES, H. A. ROWLEY, C. SACHARA, M. SOEHNGEN, S. WARACH and W. HACKE (2006): Dose Escalation of Desmoteplase for Acute Ischemic Stroke (DEDAS): evidence of safety and efficacy 3 to 9 hours after stroke onset. *Stroke* 37, 1227-1231.

GEORGE PAXINOS, C. W. (2005): *The Rat Brain in Stereotaxic Coordinates - The New Coronal Set, Fifth Edition*. Burlington, San Diego, London: Elsevier Academic Press.

GRANDIN, C. B. (2003): Assessment of brain perfusion with MRI: methodology and application to acute stroke. *Neuroradiology* 45, 755-766.

GUMBINGER, C., P. GRUSCHKA, M. BOTTINGER, K. HEERLEIN, R. BARROWS, W. HACKE and P. RINGLEB (2012): Improved prediction of poor outcome after thrombolysis using conservative definitions of symptomatic hemorrhage. *Stroke* 43, 240-242.

GURSOY-OZDEMIR, Y., A. CAN and T. DALKARA (2004): Reperfusion-induced oxidative/nitrative injury to neurovascular unit after focal cerebral ischemia. *Stroke* 35, 1449-1453.

HACKE, W., G. ALBERS, Y. AL-RAWI, J. BOGOUSSLAVSKY, A. DAVALOS, M. ELIASZIW, M. FISCHER, A. FURLAN, M. KASTE, K. R. LEES, M. SOEHNGEN and S. WARACH (2005): The Desmoteplase in Acute Ischemic Stroke Trial (DIAS): a phase II MRI-based 9-hour window acute stroke thrombolysis trial with intravenous desmoteplase. *Stroke* 36, 66-73.

HACKE, W., A. J. FURLAN, Y. AL-RAWI, A. DAVALOS, J. B. FIEBACH, F. GRUBER, M. KASTE, L. J. LIPKA, S. PEDRAZA, P. A. RINGLEB, H. A. ROWLEY, D. SCHNEIDER, L. H. SCHWAMM, J. S. LEAL, M. SOHNGEN, P. A. TEAL, K. WILHELM-OGUNBIYI, M. WINTERMARK and S. WARACH (2009): Intravenous desmoteplase in patients with acute ischaemic stroke selected by MRI perfusion-diffusion weighted imaging or perfusion CT (DIAS-2): a prospective, randomised, double-blind, placebo-controlled study. *Lancet Neurol* 8, 141-150.

HACKE, W., M. KASTE, E. BLUHMKI, M. BROZMAN, A. DAVALOS, D. GUIDETTI, V. LARRUE, K. R. LEES, Z. MEDEGHRI, T. MACHNIG, D. SCHNEIDER, R. VON KUMMER, N. WAHLGREN and D. TONI (2008): Thrombolysis with alteplase 3 to 4.5 hours after acute ischemic stroke. *N Engl J Med* 359, 1317-1329.

HACKE, W., M. KASTE, C. FIESCHI, R. VON KUMMER, A. DAVALOS, D. MEIER, V. LARRUE, E. BLUHMKI, S. DAVIS, G. DONNAN, D. SCHNEIDER, E. DIEZ-TEJEDOR and P. TROUILLAS (1998): Randomised double-blind placebo-controlled trial of thrombolytic therapy with intravenous alteplase in acute ischaemic stroke (ECASS II). Second European-Australasian Acute Stroke Study Investigators. *Lancet* 352, 1245-1251.

HADDAD, J. J. (2002): Redox regulation of pro-inflammatory cytokines and IkappaB-alpha/NF-kappaB nuclear translocation and activation. *Biochem Biophys Res Commun* 296, 847-856.

HAMANN, G. F., G. J. DEL ZOPPO and R. VON KUMMER (1999): Hemorrhagic transformation of cerebral infarction--possible mechanisms. *Thromb Haemost* 82 Suppl 1, 92-94.

HAWKINS, B. T. and T. P. DAVIS (2005): The blood-brain barrier/neurovascular unit in health and disease. *Pharmacol Rev* 57, 173-185.

HILL, M. D. and A. M. BUCHAN (2005): Thrombolysis for acute ischemic stroke: results of the Canadian Alteplase for Stroke Effectiveness Study. *CMAJ* 172, 1307-1312.

HOM, J., J. W. DANKBAAR, T. SCHNEIDER, S. C. CHENG, J. BREDNO and M. WINTERMARK (2009): Optimal duration of acquisition for dynamic perfusion CT assessment of blood-brain barrier permeability using the Patlak model. *AJNR Am J Neuroradiol* 30, 1366-1370.

HOM, J., J. W. DANKBAAR, B. P. SOARES, T. SCHNEIDER, S. C. CHENG, J. BREDNO, B. C. LAU, W. SMITH, W. P. DILLON and M. WINTERMARK (2011): Blood-brain barrier permeability assessed by perfusion CT predicts symptomatic hemorrhagic transformation and malignant edema in acute ischemic stroke. *AJNR Am J Neuroradiol* 32, 41-48.

INOUE, N., S. TAKESHITA, D. GAO, T. ISHIDA, S. KAWASHIMA, H. AKITA, R. TAWA, H. SAKURAI and M. YOKOYAMA (2001): Lysophosphatidylcholine increases the secretion of matrix metalloproteinase 2 through the activation of NADH/NADPH oxidase in cultured aortic endothelial cells. *Atherosclerosis* 155, 45-52.

JANSEN, O., P. SCHELLINGER, J. FIEBACH, W. HACKE and K. SARTOR (1999): Early recanalisation in acute ischaemic stroke saves tissue at risk defined by MRI. *Lancet* 353, 2036-2037.

JIANG, Q., R. L. ZHANG, Z. G. ZHANG, R. A. KNIGHT, J. R. EWING, G. DING, M. LU, P. ARNIEGO, L. ZHANG, J. HU, Q. LI and M. CHOPP (2002): Magnetic resonance imaging characterization of hemorrhagic transformation of embolic stroke in the rat. *J Cereb Blood Flow Metab* 22, 559-568.

KANE, I., T. CARPENTER, F. CHAPPELL, C. RIVERS, P. ARMITAGE, P. SANDERCOCK and J. WARDLAW (2007): Comparison of 10 different magnetic resonance perfusion imaging processing methods in acute ischemic stroke: effect on lesion size, proportion of patients with diffusion/perfusion mismatch, clinical scores, and radiologic outcomes. *Stroke* 38, 3158-3164.

KASSNER, A., D. M. MANDELL and D. J. MIKULIS Measuring permeability in acute ischemic stroke. *Neuroimaging Clin N Am* 21, 315-325.

KASSNER, A., D. M. MANDELL and D. J. MIKULIS (2011): Measuring permeability in acute ischemic stroke. *Neuroimaging Clin N Am* 21, 315-325.

KASSNER, A., T. ROBERTS, K. TAYLOR, F. SILVER and D. MIKULIS (2005): Prediction of hemorrhage in acute ischemic stroke using permeability MR imaging. *AJNR Am J Neuroradiol* 26, 2213-2217.

KASSNER, A., T. P. ROBERTS, B. MORAN, F. L. SILVER and D. J. MIKULIS (2009): Recombinant tissue plasminogen activator increases blood-brain barrier disruption in acute ischemic stroke: an MR imaging permeability study. *AJNR Am J Neuroradiol* 30, 1864-1869.

KIM, E. Y., S. K. LEE, D. J. KIM, S. H. SUH, J. KIM, J. H. HEO and D. I. KIM (2005): Detection of thrombus in acute ischemic stroke: value of thin-section noncontrast-computed tomography. *Stroke* 36, 2745-2747.

KIM, J. H., O. Y. BANG, D. S. LIEBESKIND, B. OVBIAGELE, G. M. KIM, C. S. CHUNG, K. H. LEE and J. L. SAVER (2010): Impact of baseline tissue status (diffusion-weighted imaging lesion) versus perfusion status (severity of hypoperfusion) on hemorrhagic transformation. *Stroke* 41, e135-142.

KISELEV, V. G. (2001): On the theoretical basis of perfusion measurements by dynamic susceptibility contrast MRI. *Magn Reson Med* 46, 1113-1122.

KNIGHT, R. A., P. B. BARKER, S. C. FAGAN, Y. LI, M. A. JACOBS and K. M. WELCH (1998): Prediction of impending hemorrhagic transformation in ischemic stroke using magnetic resonance imaging in rats. *Stroke* 29, 144-151.

KNIGHT, R. A., T. N. NAGARAJA, J. R. EWING, V. NAGESH, P. A. WHITTON, E. BERSHAD, S. C. FAGAN and J. D. FENSTERMACHER (2005): Quantitation and localization of blood-to-brain influx by magnetic resonance imaging and quantitative autoradiography in a model of transient focal ischemia. *Magn Reson Med* 54, 813-821.

KUROIWA, T., P. TING, H. MARTINEZ and I. KLATZO (1985): The biphasic opening of the blood-brain barrier to proteins following temporary middle cerebral artery occlusion. *Acta Neuropathol* 68, 122-129.

LADURNER, G., E. ZILKHA, D. ILIFF, G. H. DU BOULAY and J. MARSHALL (1976): Measurement of regional cerebral blood volume by computerized axial tomography. *J Neurol Neurosurg Psychiatry* 39, 152-158.

LANSBERG, M. G., J. LEE, S. CHRISTENSEN, M. STRAKA, D. A. DE SILVA, M. MLYNASH, B. C. CAMPBELL, R. BAMMER, J. M. OLIVOT, P. DESMOND, S. M. DAVIS, G. A. DONNAN and G. W. ALBERS (2011): RAPID automated patient selection for reperfusion therapy: a pooled analysis of the Echoplanar Imaging Thrombolytic Evaluation Trial (EPITHET) and the Diffusion and Perfusion Imaging Evaluation for Understanding Stroke Evolution (DEFUSE) Study. *Stroke* 42, 1608-1614.

LAPCHAK, P. A. (2002): Hemorrhagic transformation following ischemic stroke: significance, causes, and relationship to therapy and treatment. *Curr Neurol Neurosci Rep* 2, 38-43.

LEE, K. Y., L. L. LATOUR, M. LUBY, A. W. HSIA, J. G. MERINO and S. WARACH (2009): Distal hyperintense vessels on FLAIR: an MRI marker for collateral circulation in acute stroke? *Neurology* 72, 1134-1139.

LEV, M. H., J. FARKAS, V. R. RODRIGUEZ, L. H. SCHWAMM, G. J. HUNTER, C. M. PUTMAN, G. A. RORDORF, F. S. BUONANNO, R. BUDZIK, W. J. KOROSHETZ and R. G. GONZALEZ (2001): CT angiography in the rapid triage of patients with hyperacute stroke to intraarterial thrombolysis: accuracy in the detection of large vessel thrombus. *J Comput Assist Tomogr* 25, 520-528.

LEYS, D., J. P. PRUVO, O. GODEFROY, P. RONDEPIERRE and X. LECLERC (1992): Prevalence and significance of hyperdense middle cerebral artery in acute stroke. *Stroke* 23, 317-324.

LIN, K., K. S. KAZMI, M. LAW, J. BABB, N. PECCERELLI and B. K. PRAMANIK (2007): Measuring elevated microvascular permeability and predicting hemorrhagic transformation in acute ischemic stroke using first-pass dynamic perfusion CT imaging. *AJNR Am J Neuroradiol* 28, 1292-1298.

LONGA, E. Z., P. R. WEINSTEIN, S. CARLSON and R. CUMMINS (1989): Reversible middle cerebral artery occlusion without craniectomy in rats. *Stroke* 20, 84-91.

LYDEN, P. D. and J. A. ZIVIN (1993): Hemorrhagic transformation after cerebral ischemia: mechanisms and incidence. *Cerebrovasc Brain Metab Rev* 5, 1-16.

MARLER, J. R. and E. AL. (1995): Tissue plasminogen activator for acute ischemic stroke. The National Institute of Neurological Disorders and Stroke rt-PA Stroke Study Group. *N Engl J Med* 333, 1581-1587.

MITEFF, F., C. R. LEVI, G. A. BATEMAN, N. SPRATT, P. MCELDUFF and M. W. PARSONS (2009): The independent predictive utility of computed tomography angiographic collateral status in acute ischaemic stroke. *Brain* 132, 2231-2238.

MOLINA, C. A., J. ALVAREZ-SABIN, J. MONTANER, S. ABILLEIRA, J. F. ARENILLAS, P. COSCOJUELA, F. ROMERO and A. CODINA (2002): Thrombolysis-related hemorrhagic infarction: a marker of early reperfusion, reduced infarct size, and improved outcome in patients with proximal middle cerebral artery occlusion. *Stroke* 33, 1551-1556.

NAGARAJA, T. N., K. KARKI, J. R. EWING, R. L. CROXEN and R. A. KNIGHT (2008): Identification of variations in blood-brain barrier opening after cerebral ischemia by dual contrast-enhanced magnetic resonance imaging and T 1sat measurements. *Stroke* 39, 427-432.

NAGARAJA, T. N., K. A. KEENAN, S. L. BROWN, J. D. FENSTERMACHER and R. A. KNIGHT (2007): Relative distribution of plasma flow markers and red blood cells across BBB openings in acute cerebral ischemia. *Neurol Res* 29, 78-80.

NEUMANN-HAEFELIN, C., G. BRINKER, U. UHLENKUKEN, F. PILLEKAMP, K. A. HOSSMANN and M. HOEHN (2002): Prediction of hemorrhagic transformation after thrombolytic therapy of clot embolism: an MRI investigation in rat brain. *Stroke* 33, 1392-1398.

PATLAK, C. S. and R. G. BLASBERG (1985): Graphical evaluation of blood-to-brain transfer constants from multiple-time uptake data. Generalizations. *J Cereb Blood Flow Metab* 5, 584-590.

PATLAK, C. S., R. G. BLASBERG and J. D. FENSTERMACHER (1983): Graphical evaluation of blood-to-brain transfer constants from multiple-time uptake data. *J Cereb Blood Flow Metab* 3, 1-7.

PLANAS, A. M., S. SOLE and C. JUSTICIA (2001): Expression and activation of matrix metalloproteinase-2 and -9 in rat brain after transient focal cerebral ischemia. *Neurobiol Dis* 8, 834-846.

PLATEEL, M., E. TEISSIER and R. CECCHELLI (1997): Hypoxia dramatically increases the nonspecific transport of blood-borne proteins to the brain. *J Neurochem* 68, 874-877.

RIEDEL, C. H., P. ZIMMERMANN, U. JENSEN-KONDERING, R. STINGELE, G. DEUSCHL and O. JANSEN (2011): The importance of size: successful recanalization by intravenous thrombolysis in acute anterior stroke depends on thrombus length. *Stroke* 42, 1775-1777.

ROGER, V. L., A. S. GO, D. M. LLOYD-JONES, R. J. ADAMS, J. D. BERRY, T. M. BROWN, M. R. CARNETHON, S. DAI, G. DE SIMONE, E. S. FORD, C. S. FOX, H. J. FULLERTON, C. GILLESPIE, K. J. GREENLUND, S. M. HAILPERN, J. A. HEIT, P. M. HO, V. J. HOWARD, B. M. KISSELA, S. J. KITTNER, D. T. LACKLAND, J. H. LICHTMAN, L. D. LISABETH, D. M. MAKUC, G. M. MARCUS, A. MARELLI, D. B. MATCHAR, M. M. MCDERMOTT, J. B. MEIGS, C. S. MOY, D. MOZAFFARIAN, M. E. MUSSOLINO, G. NICHOL, N. P. PAYNTER, W. D. ROSAMOND, P. D. SORLIE, R. S. STAFFORD, T. N. TURAN, M. B. TURNER, N. D. WONG and J. WYLIE-ROSETT (2011): Heart disease and stroke statistics--2011 update: a report from the American Heart Association. *Circulation* 123, e18-e209.

ROSELL, A., A. ORTEGA-AZNAR, J. ALVAREZ-SABIN, I. FERNANDEZ-CADENAS, M. RIBO, C. A. MOLINA, E. H. LO and J. MONTANER (2006): Increased brain expression of matrix metalloproteinase-9 after ischemic and hemorrhagic human stroke. *Stroke* 37, 1399-1406.

ROSEN, B. R., J. W. BELLIVEAU, J. M. VEVEA and T. J. BRADY (1990): Perfusion imaging with NMR contrast agents. *Magn Reson Med* 14, 249-265.

ROSENBERG, G. A., M. NAVRATIL, F. BARONE and G. FEUERSTEIN (1996): Proteolytic cascade enzymes increase in focal cerebral ischemia in rat. *J Cereb Blood Flow Metab* 16, 360-366.

ROUCHAUD, A., M. MAZIGHI, J. LABREUCHE, E. MESEGUER, J. M. SERFATY, J. P. LAISSY, P. C. LAVALLEE, L. CABREJO, C. GUIDOUX, B. LAPERGUE, I. F. KLEIN, J. M. OLIVOT, H. ABBOUD, O. SIMON, E. SCHOUMAN-CLAEYS and P. AMARENCO (2011): Outcomes of mechanical endovascular therapy for acute ischemic stroke: a clinical registry study and systematic review. *Stroke* 42, 1289-1294.

ROWLEY, H. A. (2001): The four Ps of acute stroke imaging: parenchyma, pipes, perfusion, and penumbra. *AJNR Am J Neuroradiol* 22, 599-601.

SAHA, G. B., W. J. MacIntyre and R. T. Go (1994): Radiopharmaceuticals for brain imaging. *Semin Nucl Med* 24, 324-349.

SANAK, D., V. Nosal, D. Horak, A. Bartkova, K. Zelenak, R. Herzig, J. Bucil, D. Skoloudik, S. Burval, V. Cisarikova, I. Vlachova, M. Kocher, J. Zapletalova, E. Kurca and P. Kanovsky (2006): Impact of diffusion-weighted MRI-measured initial cerebral infarction volume on clinical outcome in acute stroke patients with middle cerebral artery occlusion treated by thrombolysis. *Neuroradiology* 48, 632-639.

SAVER, J. L. (2007): Hemorrhage after thrombolytic therapy for stroke: the clinically relevant number needed to harm. *Stroke* 38, 2279-2283.

SCHELLINGER, P. D., R. N. Bryan, L. R. Caplan, J. A. Detre, R. R. Edelman, C. Jaigobin, C. S. Kidwell, J. P. Mohr, M. Sloan, A. G. Sorensen and S. Warach (2010): Evidence-based guideline: The role of diffusion and perfusion MRI for the diagnosis of acute ischemic stroke: report of the Therapeutics and Technology Assessment Subcommittee of the American Academy of Neurology. *Neurology* 75, 177-185.

SCHELLINGER, P. D., J. A. Chalela, D. W. Kang, L. L. Latour and S. Warach (2005): Diagnostic and prognostic value of early MR Imaging vessel signs in hyperacute stroke patients imaged <3 hours and treated with recombinant tissue plasminogen activator. *AJNR Am J Neuroradiol* 26, 618-624.

SCHLAUG, G., A. Benfield, A. E. Baird, B. Siewert, K. O. Lovblad, R. A. Parker, R. R. Edelman and S. Warach (1999): The ischemic penumbra: operationally defined by diffusion and perfusion MRI. *Neurology* 53, 1528-1537.

SCHNEIDER, T., J. Hom, J. Bredno, J. W. Dankbaar, S. C. Cheng and M. Wintermark (2011): Delay correction for the assessment of blood-brain barrier permeability using first-pass dynamic perfusion CT. *AJNR Am J Neuroradiol* 32, E134-138.

SHOBHA, N., A. M. Buchan and M. D. Hill (2011): Thrombolysis at 3-4.5 hours after acute ischemic stroke onset--evidence from the Canadian Alteplase for Stroke Effectiveness Study (CASES) registry. *Cerebrovasc Dis* 31, 223-228.

SMITH, A. M., C. B. Grandin, T. Duprez, F. Mataigne and G. Cosnard (2000): Whole brain quantitative CBF and CBV measurements using MRI bolus tracking: comparison of methodologies. *Magn Reson Med* 43, 559-564.

SMITH, W. S., G. SUNG, J. SAVER, R. BUDZIK, G. DUCKWILER, D. S. LIEBESKIND, H. L. LUTSEP, M. M. RYMER, R. T. HIGASHIDA, S. STARKMAN, Y. P. GOBIN, D. FREI, T. GROBELNY, F. HELLINGER, D. HUDDLE, C. KIDWELL, W. KOROSHETZ, M. MARKS, G. NESBIT and I. E. SILVERMAN (2008): Mechanical thrombectomy for acute ischemic stroke: final results of the Multi MERCI trial. *Stroke* 39, 1205-1212.

SMITH, W. S., G. SUNG, S. STARKMAN, J. L. SAVER, C. S. KIDWELL, Y. P. GOBIN, H. L. LUTSEP, G. M. NESBIT, T. GROBELNY, M. M. RYMER, I. E. SILVERMAN, R. T. HIGASHIDA, R. F. BUDZIK and M. P. MARKS (2005): Safety and efficacy of mechanical embolectomy in acute ischemic stroke: results of the MERCI trial. *Stroke* 36, 1432-1438.

SOOD, R., Y. YANG, S. TAHERI, E. CANDELARIO-JALIL, E. Y. ESTRADA, E. J. WALKER, J. THOMPSON and G. A. ROSENBERG (2009): Increased apparent diffusion coefficients on MRI linked with matrix metalloproteinases and edema in white matter after bilateral carotid artery occlusion in rats. *J Cereb Blood Flow Metab* 29, 308-316.

TAN, J. C., W. P. DILLON, S. LIU, F. ADLER, W. S. SMITH and M. WINTERMARK (2007): Systematic comparison of perfusion-CT and CT-angiography in acute stroke patients. *Ann Neurol* 61, 533-543.

THOMALLA, G., B. CHENG, M. EBINGER, Q. HAO, T. TOURDIAS, O. WU, J. S. KIM, L. BREUER, O. C. SINGER, S. WARACH, S. CHRISTENSEN, A. TRESZL, N. D. FORKERT, I. GALINOVIC, M. ROSENKRANZ, T. ENGELHORN, M. KOHRMANN, M. ENDRES, D. W. KANG, V. DOUSSET, A. G. SORENSEN, D. S. LIEBESKIND, J. B. FIEBACH, J. FIEHLER and C. GERLOFF (2011): DWI-FLAIR mismatch for the identification of patients with acute ischaemic stroke within 4.5 h of symptom onset (PRE-FLAIR): a multicentre observational study. *Lancet Neurol* 10(11), 978-986.

VIDARSSON, L., R. E. THORNHILL, F. LIU, D. J. MIKULIS and A. KASSNER (2009): Quantitative permeability magnetic resonance imaging in acute ischemic stroke: how long do we need to scan? *Magn Reson Imaging* 27, 1216-1222.

WANG, X. and E. H. LO (2003): Triggers and mediators of hemorrhagic transformation in cerebral ischemia. *Mol Neurobiol* 28, 229-244.

WARDLAW, J. M. and O. MIELKE (2005): Early signs of brain infarction at CT: observer reliability and outcome after thrombolytic treatment--systematic review. *Radiology* 235, 444-453.

WINTERMARK, M., P. MAEDER, J. P. THIRAN, P. SCHNYDER and R. MEULI (2001): Quantitative assessment of regional cerebral blood flows by perfusion CT studies at low injection rates: a critical review of the underlying theoretical models. *Eur Radiol* 11, 1220-1230.

WINTERMARK, M., M. REICHHART, J. P. THIRAN, P. MAEDER, M. CHALARON, P. SCHNYDER, J. BOGOUSSLAVSKY and R. MEULI (2002): Prognostic accuracy of cerebral blood flow measurement by perfusion computed tomography, at the time of emergency room admission, in acute stroke patients. *Ann Neurol* 51, 417-432.

WINTERMARK, M., M. SESAY, E. BARBIER, K. BORBELY, W. P. DILLON, J. D. EASTWOOD, T. C. GLENN, C. B. GRANDIN, S. PEDRAZA, J. F. SOUSTIEL, T. NARIAI, G. ZAHARCHUK, J. M. CAILLE, V. DOUSSET and H. YONAS (2005): Comparative overview of brain perfusion imaging techniques. *Stroke* 36, e83-99.

YOO, A. J., L. A. VERDUZCO, P. W. SCHAEFER, J. A. HIRSCH, J. D. RABINOV and R. G. GONZALEZ (2009): MRI-based selection for intra-arterial stroke therapy: value of pretreatment diffusion-weighted imaging lesion volume in selecting patients with acute stroke who will benefit from early recanalization. *Stroke* 40, 2046-2054.